Applied Water Science (2023) 13:78
https://doi.org/10.1007/s13201-023-01880-y

ORIGINAL ARTICLE

Magnetite-impregnated biochar of parthenium hysterophorus for adsorption of Cr(VI) from tannery industrial wastewater

Jemal Fito[1] · Mikiyas Abewaa[2] · Thabo Nkambule[1]

Received: 15 November 2022 / Accepted: 18 January 2023

Abstract

The tannery industry inevitably generates toxic and catastrophic wastewater, which results in a huge threat to public health and water resources. Therefore, this work aimed to synthesize parthenium hysterophorus-based biochar–Fe_3O_4 composite for removal of Cr(VI) from tannery wastewater under 3^4 full factorial experimental designs of the Box–Behnken, which was analyzed using response surface methodology under four independent factors of pH (3, 6, and 9), initial Cr(VI) concentrations (40, 70, and 100 mg/L), contact times (30, 60, and 90 min), and adsorbent doses (20, 60, and 100 mg/100 mL). This composite adsorbent was described by a high BET surface area of 237.4 m^2/g, XRD prominent peaks, SEM morphology corroborate and FTIR multifunctionalities of O–H at 3296 cm^{-1}, the vibration of ketone C–OH at 1240 cm^{-1}, and the vibration of C–O–C at 1147 cm^{-1} and Fe–O stretching at 542 cm^{-1}. The maximum Cr(IV) removal efficiency of 91.8% was recorded at an initial Cr(VI) concentration of 40 mg/L, pH of 3, adsorbent dose of 100 mg/100 mL, and a contact time of 90 min, whereas the minimum Cr(VI) removal of 17.3% was observed at an initial Cr(VI) concentration of 100 mg/L, 20 mg/100 mL of adsorbent dose, pH of 9, and contact time of 30 min. The concentration of Cr(VI) in real wastewater was determined to be 85.13 mg/L and its remediation was found to be 81.8%. Langmuir's model was the best fit with experimental data at R^2 0.99 and q_{max} 400 mg/g, showing that the adsorption process was homogenous and monolayer. In conclusion, the adsorption results were encouraging, and biochar–Fe_3O_4 appears to be a potential candidate for Cr removal from wastewater.

Keywords Coprecipitation · Effluent · Heavy metal · Magnetite adsorbent · Treatment · Water pollution

Introduction

The current global water demand and discrepancy are increasing geometrically and are anticipated to reach 20–30% and 55% by 2050, respectively (Burek et al. 2016; UN-water 2021; Moges et al. 2022). Water quantity and quality are cross-cutting issues in all sustainable development goals. Goal 6 of sustainable development (agenda 2030) stated clean, safe, sufficient, and affordable water for all of humanity. However, 40% of the global population will face water scarcity (1000 m^3) and stress (1000–1700 m^3) per person per year by 2030 and 4.8–5.7 billion people will be at risk by 2050 (WWAP/UN-Water 2017; UN-water 2021). Practically, water resource conservation, development, and water reuse are potential candidates to mitigate water stress and enhance sustainability. Particularly, wastewater reclamation and reuse are compulsory strategies to protect against water pollution and tackle water stress. But, more than 80% of global wastewater is discharged without adequate treatment (UN-Water 2020). The contribution of industrial wastewater to environmental pollution is significant. The tannery industry is found as the frontline contributor to water pollution. About 300 million tons of tannery wastewater are generated every year across the world (Zhao and Chen 2019). Globally, the leather industry is one of the classical and largest manufacturing sectors which generates inevitably toxic wastewater (Cheng et al. 2021b). Wastewater in leather industries is generated from five process units such as washing, liming and unhairing, chrome tanning, degreasing, and fatliquoring and dyeing. Normally, the major pollutants in tannery industrial wastewater are chlorides, nitrogen,

✉ Mikiyas Abewaa
mikiyasabewaa02@gmail.com

[1] Institute for Nanotechnology and Water Sustainability (iNanoWS), College of Science, Engineering and Technology, University of South Africa, Florida Science Campus, Johannesburg 1710, South Africa

[2] Department of Environmental Engineering, Addis Ababa Science & Technology University, Addis Ababa, Ethiopia

Published online: 09 February 2023

sulfates, sulfides, BOD_5, COD, Cr, and suspended solids (Doumbi et al. 2022).

Chromium is the most toxic and abundant pollutant in tannery wastewater because chromium salts are the major consumable chemical in the leather tanning process in 90% of leather industries worldwide (Shan et al. 2021). Globally, about 90% of leather products are produced using the chrome tanning method (Sathish et al. 2019). The tannage process is the most commonly used technique in the leather industry (Liu et al. 2022). Chrome tanning is highly associated with severe environmental pollution (Zhou et al. 2022). Additionally, the harmful chemicals that are commonly used in the tanning process and contributed to tannery wastewater toxicity are surface-active compounds, grease, azo dyes, sulphonated oils, pthalates, organic chemicals (tannins), and phenolic compounds (Yadav et al. 2019). Chromium fixation in the tanning process was 60–70%, but the weight of Cr to hides is about 2% (Nur-E-Alam et al. 2018). The chemistry of Cr in water and wastewater is complex and its long-run impact on the environment is severe. Specifically, Cr is a highly noxious trace element that exists in water in the form of chromate (CrO_4^{2-}, $Cr(OH)^{2+}$, $Cr(OH)_3$, and $Cr(OH)_4$) and dichromate ($Cr_2O_7^{2-}$, $HCrO_4^-$, and CrO_4^{2-}) (Huang et al. 2018; Aigbe and Osibote 2020). Essentially, Cr is a toxic (genotoxicity, phytotoxicity, and cytotoxicity) and hazardous chemical that can cause chronic health problems such as mutagenic, carcinogenic, skin irritation, lung cancer, kidney dysfunction, liver failure, anemia, diarrhea, and vomiting (Preethi et al. 2017; Huang et al. 2018; Yadav et al. 2019; Kong et al. 2021). The toxicity of Cr(VI) is 500 times more harmful than Cr (III)(Zhao and Chen 2019). Generally, Cr is a harmful chemical that can cause severe threats to human health, aquatic life, and water resources (Aigbe and Osibote 2020). Hence, Cr removal from tannery wastewater is a very urgent and sensitive agendum to protect the public and the environment.

The performance of treatment technologies for Cr removal is inconsistent and insignificant across the globe (Kosek et al. 2020). The challenge of achieving green and sustainable development in the leather industry is highly attributed to inadequately treated wastewater. The stringent quality standard of Cr concentration has already been in place. For instance, the maximum Cr concentration in drinking water is 0.05 mg/L, and the concentration of Cr that should be discharged in water bodies is 50 mg/L (Parlayici et al. 2015; Huang et al. 2018; Aigbe and Osibote 2020). Then, the removal of Cr from the wastewater is indispensable both legally and morally to protect environmental pollution and public health. But, the performance of conventional wastewater treatment plant for Cr removal is still inefficient and remains problematic. However, advanced wastewater treatment technologies such as chemical precipitation, advanced oxidation process, adsorption, solvent extraction, electrocoagulation, membrane separation processes, coagulation/flocculation, electro-Fenton processes, reverse osmosis, ion exchange, and electrodialysis have been applied for remediation of tannery wastewater (Huang et al. 2018; Enaime et al. 2020; Fito et al. 2020a; Hansen et al. 2021; Doumbi et al. 2022; Villaseñor-Basulto et al. 2022). But, these technologies have certain limitations including excessive expensiveness, the inability to comply with standards, scale-up issues, fouling, short service life, complex preparation steps, high reagent consumption, environmental compatibility, longer reactions, and energy intensiveness (Huang et al. 2018). However, adsorption is the most superior and promising technology among the groups (Mallik et al. 2021; Tebeje et al. 2021). This technology is practically manageable, economically variable, technically flexible, technologically feasible, and environmentally friendly.

Various adsorbent materials are used in the adsorption process of water and wastewater treatment. Recently, adsorbents are categorized into major classes such as biomaterials, zeolite, metal (oxides), clay minerals, and activated carbon (Neolaka et al. 2020; Sirajudheen et al. 2020). Plenty of the local and low-cost adsorbents are prepared from different kinds of materials such as cassava peel, willow peat, bamboo, bagasse fly ash, cotton, walnut shells, pine tar, orange peel, miscanthus straw, agricultural wastes, orange waste, the bark of the Vitex negundo morinda, tinctorial bark, bagasse, avocado seed, wheat straw, watermelon rinds, zeolites, clay minerals, sludge, macro-algae, parthenium hysterophorus, sawdust, buffalo weed, wood pellets, ramie bars, hemp stem, reed straw, coconut husks, and crocus sativus leaves (Lingamdinne et al. 2015, 2022; Roh et al. 2015; Mishra et al. 2019; Fito et al. 2020a; Lee and Park 2020; Neolaka et al. 2020; Sirajudheen et al. 2020; Xiao et al. 2021; Tebeje et al. 2021; Narasimharao et al. 2023). However, the application of these technologies is limited due to weak adsorbent regeneration, practical challenges, poor sludge management, and low treatment efficiency (Moges et al. 2022). Hence, the scientific community is striving to research potential adsorbents which can replace the efficient and expensive commercial activated carbon. In line with this, biochar emerges as a promising adsorbent for the remediation of water and wastewater. Biochar has the advantages of being a highly porous, versatile catalyst and has flexible architecture, high surface area, easily functionalized surface, low cost, stable carbon matrix, and available feedstock (Vikrant et al. 2018; Fito et al. 2022). Moreover, biochar is composed of persistent free radicals which are an essential component to generate the hydroxyl radicals to enhance photocatalytic activity (Lyu et al. 2020). The potential of various biochars for the removal of heavy metals including Cr was investigated and promising results have been reported (Agra et al. 2014; Shang et al. 2016; Zhu et al. 2018; Regkouzas and Diamadopoulos 2019; Gupta et al. 2020). Biochar

adsorption mechanisms can be either physical or chemical interactions such as ion exchange, precipitation, surface and inner-sphere complexation, electrostatic attraction, and redox (Zhang et al. 2020). However, the major limitations of pristine biochar adsorption are the inability to adsorb numerous anions, aggregation, poor mechanical characteristics, and suspension due to low density. Therefore, surface modification and multifunctionalities of biochar enhance the adsorption performances. In agreement with this, the presence of oxygen-containing functional groups on biochar such as C–O of phenol, alcohol, ether, and C = O of ketone or aldehyde reduced Cr(VI) from 24.4–9.65% to a less toxic form (Lyu et al. 2020).

Nowadays, composite adsorbents have emerged as an alternative method to mitigate the limitations of pristine biochar materials. Particularly, incorporating magnetite (iron oxide, Fe_3O_4) into biochar has many advantages. Magnetite has excellent superparamagnetic properties, suitability, and non-toxic nature (Zahid et al. 2019; Sirajudheen et al. 2020). Incorporating ferrites in biochar may have improved functionalities, structure, active sites and mechanical, thermal, optical, magnetic, and electric properties (Wang and Wang 2019; Tariq et al. 2020; Cheng et al. 2021a; Zubair et al. 2021; Moges et al. 2022). Additionally, magnetite is useful to tackle the problem of sludge separation of post-wastewater treatment. Biochar–ferrites composite can offer dual benefits of adhering and degradation in cleaning up water and wastewater (Yu et al. 2018). The application of such composite adsorbent in water and wastewater treatment enhances adsorption performance and shortens reaction time (Yousefi et al. 2016, 2017, Yousefi et al. 2019a, Yousefi et al. 2019b, Yousefi et al. 2021c, Yousefi et al. 2021a, Yousefi et al. 2021b; Ghasemabadi et al. 2018; Subedi et al. 2019; Karamipour et al. 2020). For instance, magnetic biochar is more effective compared with pristine biochar in the removal of tetracycline, phosphate, methylene blue, pesticide, and heavy metals (Cu(II), Cd(II), Pb(II), and Zn(II)) (Li et al. 2020b; Fuat and Cumali 2021). Moreover, promising Cr(VI) removal efficiencies of 142.9 ± 0.9 mg/g (293 K), 151 ± 1 mg/g (303 K), and 164 ± 2 mg/g (313 K) at pH 2) have been reported (Huang et al. 2018). Successful preparation of activated carbon from the parthenium hysterophorus plant was reported and its potential for industrial wastewater treatment has been tested (Bedada et al. 2020; Fito et al. 2020a). But, the study of parthenium hysterophorus-based biochar–ferrite composite for water and wastewater treatment under various surface functionalities, composite, preparation methods, and adsorption optimization was limited in literature. Therefore, this study aimed to evaluate the performance of parthenium hysterophorus-based biochar–Fe_3O_4 composite for removal of chromium from tannery industrial wastewater using 3^4 full factorial experimental designs at four factors and three levels (initial Cr(VI) concentration, pH, contact time, and adsorbent dose). Optimization and interactions of the adsorption process were performed using a response surface methodology intended to reduce the cost, number of experiments, and time. Finally, the linear regression model was used to investigate the interaction effect on adsorption processes.

Materials and methods

Tannery wastewater sampling and characterization

Tannery wastewater samples were collected from the Batu tannery factory in Addis Ababa city which is located on the east bank of the little Akaki River in the Kality area. This factory is found at the geographical coordinate of 8° 55′54" N and 38° 45′29" E) which is indicated in Fig. 1. Batu tannery factory is a private limited company and was founded in 1992. This factory has a total initial capital of birr 22,000,000. The company has an input capacity of 1200 full hides, 30,000 sqft/day, producing around 40,000 sqft of retaining and dyeing, and a 45,000-finishing capacity. The daily processing capacity of the tannery is 1000 goat skins, 3000 sheepskins, and 1200 cowhides. Moreover, the tannery produces products that are specifically designed for production of high-quality products. These products including footwear uppers, gloves, purses, luggage, garments, and belts are in considerable demand among major Asian and European purchasers. Currently, the company is more focused on cowhides and 50% of finished leather products are distributed to local shoe and bag manufacturing companies. Batu tannery industry wastewater is drained out, usually into the Akaki–Kality River, and collected along with household effluent in the same drain channel. The company received ISO 9001:2015 certification in 2017.

A composite sampling technique was used to get a representative effluent sample in terms of quality. The samples were collected in polyethylene plastic bottles. These bottles were washed with detergent and diluted HCl. Finally, it was repeatedly rinsed with distilled deionized water. The physicochemical parameters of wastewater and the corresponding testing method used in this analysis are summarized in Table 1. Wastewater sampling was duplicated and the average results of tannery wastewater characterization were reported (Waktole et al. 2019; Bedada et al. 2020; Yehuala et al. 2021; Moges et al. 2022).

Adsorbent preparation

Preparation of biochar

Parthenium hysterophorus is a weed plant in Ethiopia found everywhere in the central part of the country. The

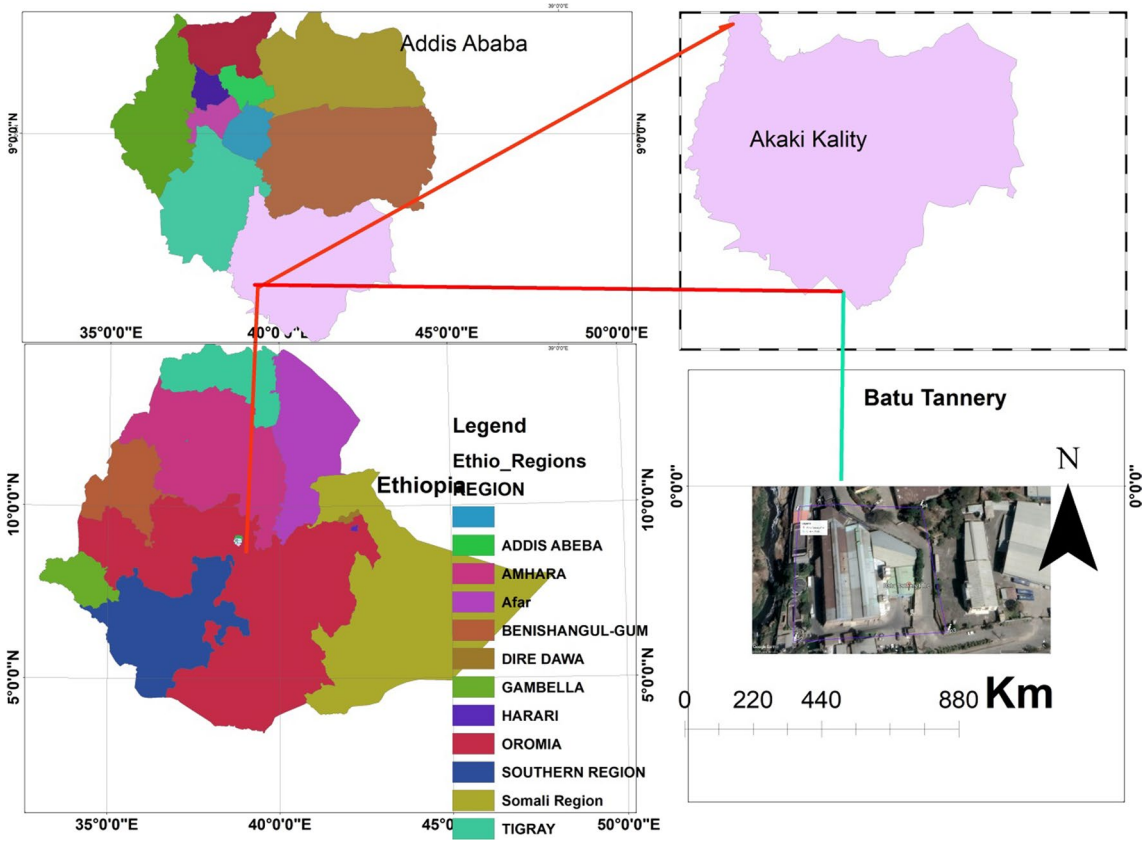

Fig. 1 The location of the wastewater sampling site of the Batu Tannery factory

Table 1 Testing methods for physicochemical parameters of tannery wastewater

S. no	Parameters	The specific method for each parameter
1	pH	Hach HQD field case, model 58, 258–00
2	Temperature	Hach photometer HQD field case, model 58, 258–00
3	EC	Hach photometer HQD field case, model 58, 258–00
4	COD	APHA 5220 B, open reflux method
5	TS	APHA 5220 B, total solid dried at 103–105 °C
6	Cr(VI)	APHA 3120 B
7	Phosphate	APHA 5220 B, Vanadomolybdophosphoric acid
8	Sulfate	APHA 5220 B, turbidmetric method
9	BOD_5	APHA 5210 B, 5-day BOD test

plant sample was collected from the Addis Ababa Science and Technology University premise which is situated in the capital city of the country. The geographical coordinate of the sampling site is 8° 58′ N and 38° 47′ E at a high altitude of 2300 m above sea level. This is described by the relative humidity of 60.7% and rainfall of 1089 mm with an annual mean temperature of 15.9 °C. Parthenium hysterophorus samples were chopped into 5–10 mm sizes and were washed with distilled water to remove the dust particles. This chopped material was placed in an appropriate container and dried in an oven at 105 °C for 24 h. Then, the dried sample was pyrolyzed in a fume furnace at a fixed temperature of 500 °C for 2 h. The charred adsorbent was cooled, weighed, and placed in a tightly sealed desiccator (Bedada et al., 2020a; Fito et al. 2020a; Chen et al. 2021a, b; Qhubu et al. 2021; Qu et al. 2021; Wan et al. 2021; Moges et al. 2022). Figure 2 depicts the most essential steps of biochar preparation.

Magnetite preparation

Chemical coprecipitation is the most promising method for producing nanoparticles due to its ease of implementation and less hazardous chemical and procedure requirements. There are two main methods for coprecipitation synthesis in the solution of spherical magnetic nanoparticles. The first method involves the partial oxidation of ferrous hydroxide suspensions followed by coprecipitation. The other method involves aging stoichiometric mixtures of ferrous and ferric hydroxides in an aqueous solution, yielding magnetic nanoparticles (Zhang et al. 2017; Dudchenko et al. 2022; Niculescu et al. 2022). For this study, the coprecipitation

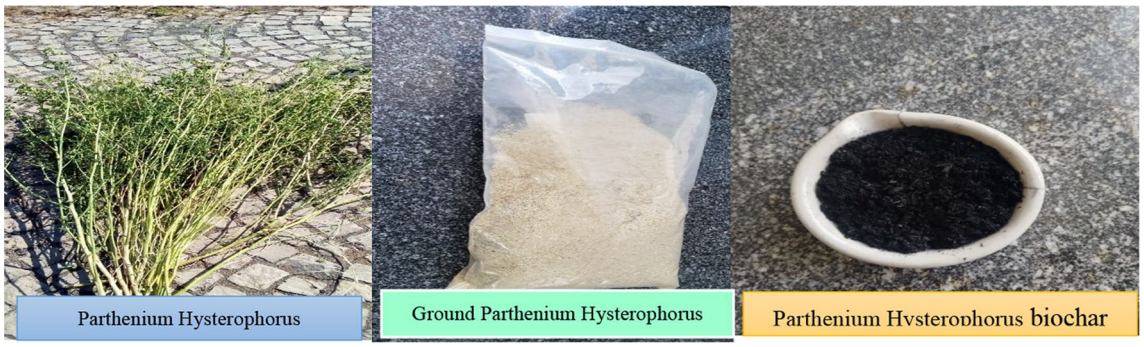

Fig. 2 Preparation steps of parthenium hysterophorus biochar

method was used for the synthesis of magnetite. In this process, 3.3 g $FeSO_4 \bullet 7H_2O$ and 2 g of $NaNO_3$ were dissolved in 50 mL of distilled water as shown in Fig. 3. The pH of this solution was adjusted between 9 and 14 using a 2.5-M NaOH solution. Then, the mixture was heated to 80 °C. The precipitation was enhanced through continuous string at the same temperature. The solution was cooled down to room temperature for 30 min. The formulated precipitate of the solution was filtered using Whatman filter paper 42 and washed several times with distilled water to remove unwanted chemicals on the crystalline particles. The precipitate of magnetite particles was then oven dried at a temperature of 60 °C overnight before being coated with biochar. Finally, the magnetic properties of the magnetite were checked using external magnetic substances (Alzahrani 2017; Frolova 2019; Moges et al. 2022).

Biochar–ferrite composite preparation

The intention of anchoring ferrites to biochar is to acquire an appropriate surface structure, good magnetic properties, high surface area, high adsorption capacity, and reusability. The qualities of composites and performance depend on the method used and the ratios of spinel to biochar (Fito et al. 2022). The most commonly used techniques for magnetic biochar synthesis are coprecipitation, calcination, pyrolysis, oxidative hydrolysis, thermochemical techniques (pyrolysis and calcination), and mechanical milling (Li et al. 2020b; Rocha et al. 2020; Fito et al. 2022). However, coprecipitation is the most widely used technique employed for magnetic biochar synthesis and magnetite was deposited on the surface of the biochar (Fito et al. 2022). In this approach, a beaker was filled with 2:1 (w/w) of biochar to magnetite in 100 mL of distilled water (Alam et al. 2020). The mixture was heated to 65 °C after being stirred. The pH of the solution of precipitate iron hydroxides was adjusted using 5 M NaOH solution in the range of 10–11 by adding drop by drop. This solution was mixed continuously for 1 h and before decanting overnight. Then, after the supernatant was removed, the precipitates were filtered, washed, rinsed with de-ionized water, and dried in an oven at 80 °C (Bhushan et al. 2020; Ameen et al. 2021). Finally, the biochar–ferrite composite was ground into 250 μm particle sizes and stored in an airtight plastic bag until it was utilized for treatments as illustrated in Fig. 4 (Fito et al. 2020a; Moges et al. 2022).

Adsorbent characterization

Proximate analysis

All the proximal parameters such as ash content, moisture content, volatile matter, and fixed carbon of biochar ferrite were determined using conventional American Society for Testing and Materials (ASTM) procedures. The moisture content was calculated using Eq. 1. A sample of 1.0 g was placed in the crucible and then heated in an oven at 105 °C

Fig. 3 Steps of synthesizing magnetite particles

Fig. 4 The steps of preparation of biochar–magnetite composite

for 4 h at a constant temperature. Similarly, for volatile matter, 1 g of biochar–ferrite composite was placed in a preheated crucible and heated in a muffle furnace at 800 °C for 8 min under standardized circumstances with no contact with air (Eq. 2). The ash content was determined by placing 1 g of adsorbent in preheated crucibles in the furnace which was heated at 500 °C for 4 h (Eq. 3). Finally, the fixed carbon (FC) of the adsorbent was calculated by subtracting the sum of the percentages of moisture content, ash content, and volatile matter content from 100 as indicated in Eq. 4 (Fito et al. 2019b, 2020a; Bedada et al. 2020).

$$MC = \left(\frac{W_1 - W_2}{W_1}\right)100\% \tag{1}$$

$$VM = \left(\frac{W_1 - W_2}{W_1}\right)100\% \tag{2}$$

$$AC = \left(\frac{W_2}{W_1}\right)100\% \tag{3}$$

$$FC(\%) = 100 - (MC + VM + AC) \tag{4}$$

where W_1 represents adsorbent weight before heating, W_2 is the weight after ignition, VM is the volatile matter, AC is the ash content, FC is the fixed carbon, and MC is the moisture composition of biochar ferrite (Nure et al. 2017).

Zero-point of charge (pH_{pzc})

The pH of wastewater significantly influences the adsorption of various contaminants. It also affects the ionization of chemically active sites on adsorbent. For particular temperature, pressure, and aqueous solution components, the pH of the point of zero charges (pH_{pzc}) is the value of pH at which the net surface charge is equal to zero. At pH equal to pH_{pzc}, the solution becomes neutral which equals amounts of negative and positive charges. Acid–base titration and mass titration are some of the methods used to determine pH_{pzc}. For this work, the pH_{pzc} of biochar–ferrite was determined by employing the mass titration method. Normally, this method is found to be simple and straightforward with adequate results (Kosmulski 2020). In this process, 1 g of biochar–ferrite adsorbent was added to six Erlenmeyer flasks containing 50 mL of 0.1 M NaCl. The pH of the solutions varied between 2 and 12 using 0.1 M NaOH or 0.1 M HCl. Finally, after 48 h, the pH of the solution was measured, and pH_{pzc} was determined from the point where the pH final and pH initial curves overlapped (Hoang et al. 2019, 2020; Tebeje et al. 2021).

SEM, FTIR, XRD, and BET analyses

Scanning electron microscopy was used to examine the surface morphology of biochar–ferrite adsorbent. The sample preparation and scanning were carried out according to the machine's regular operating protocols. The analysis was carried out with a 10 μm resolution and a guaranteed capacity of 10 kV. The machine used for the analysis was JCM-6000PLUS BENCHTOP SEM, JOEL, Japan. The adsorbent sample was placed on the carbon tape and the machine was run at an 8-mm working distance. The SEM was operated at a probe current of 10 A and operating energy of 10 kV with a magnification of 1000 times (Fito et al. 2017, 2020b; Bedada et al. 2020; Yehuala et al. 2021; Moges et al. 2022). Functional groups present on the biochar ferrite were identified using infrared Fourier transform (FTIR). In this process, the biochar–ferrite composite was mixed thoroughly with dry KBr at the ratio of 2:200. Then, the sample was crushed in a mortar to produce a homogenous powder combination, which was then injected into a molder to produce a very fine plate. The FTIR spectrophotometer (FTIR, Thermo Nicolet 5700, and Waltham, MA, USA) was subsequently used to perform the plate analysis. Then, the adsorbent spectra were examined at 4000–400 cm^{-1} (Fito et al. 2017, 2020b;

Bedada et al. 2020; Yehuala et al. 2021; Moges et al. 2022). Finally, the FTIR data graph was presented using Origin Pro version 10. Similarly, the specific surface area was determined under a vacuum at 200 °C working temperature for 1 h. The sample biochar–ferrite adsorbent of 0.4 g was placed in three preparation tubes. The specific surface area of the adsorbent was calculated based on the isotherms of adsorption and desorption of nitrogen gas at 700 mm atmospheric pressure. The adsorption of N_2 on the surface of the adsorbent was performed using liquid nitrogen at − 196.5 °C. The BET-specific surface area of the adsorbent was calculated using the p/p0 ratio (Tebeje et al. 2021; Moges et al. 2022). Finally, the crystalline structure of biochar ferrite was determined using X-ray diffraction (XRD). This is a powerful non-destructive technique that identifies the existence of crystalline minerals in a given sample. The machine used for the analysis was an X-ray powder diffraction (XRD) instrument (XRD-X-ray tube Cu 40 kv, 40 mA, Olympus BTXH). X-ray diffractograms analysis was undertaken with Cu-Kα radiation ($\lambda = 0.15406$), accelerating maximum voltage (40 kV), the current intensity of (30 mA), and scanning speed of 80°/min in the range of $2\theta = 2–80°$ sampling pitch of 0.0200°. The analysis was performed under the conditions of initialization power of 15 kV, 5 mA, and a fixed wavelength of 1.541 nm. Finally, the observed peaks were used to determine the crystalline structure of the sample (Aryee et al. 2021; Tebeje et al. 2021; Bekhoukh et al. 2022; Moges et al. 2022).

Chromium adsorption optimization

The batch adsorption experiment was performed on both synthetic and real wastewater. Cr(VI) stock solution was prepared by dissolving 2.83 g analytical-grade $K_2Cr_2O_7$ in 1000 mL distilled water to obtain 1000 mg/L of Cr(VI) synthetic solution. The stock solution was diluted further with distilled water to obtain the necessary concentration of the working solutions. Then, the three chromium solutions (100 mg/L, 70 mg/L, and 40 mg/L) were prepared from the stock solution of 1000 mg/L. The pH of solutions was adjusted using 0.1 M HCl or NaOH depending on the alkalinity or acidity of the sample solution (Baird et al., Zhao et al. 2012; Badessa et al. 2020; Moges et al. 2022). The adsorption experiment was conducted using predetermined experimental conditions where the adsorbate and adsorbent were filled in volumetric flasks containing 100 mL mixtures. Each flask's solution was stirred at 125 rpm using an orbital shaker, and the solution was separated with Whatman filter paper 42. The filtrates were then collected in various sampling bottles, and the efficiency of chromium removal was determined using a UV-visible spectrophotometer (Agilent technology, Cary 100 UV–visible Spectrophotometer) after reaction with 1.5-diphenyl carbazide. The reagent of 0.25 g diphenyl carbazide was dissolved in 25 mL of acetone and mixed until completely dissolved. The solution was then made up of deionized water to a final volume of 50 mL. The calibration curve was drawn using the absorbance of known Cr(VI) concentrations of 20, 40, 60, 80, and 100 mg/L. The linear graph of absorbance against concentration approaches was recorded and the unknown Cr(VI) concentrations were determined based on the Beer–Lambert equation (Bedada et al. 2020; Moges et al. 2022). The response variable of chromium removal was recorded as a dependent variable, whereas the three experimental factors with four levels (contact time, initial chromium concentration, pH, and adsorbent dosage) were used in the study as indicated in Table 2. The values of adsorption factors were set based on previous studies. The regression model and response surface methods were used to evaluate the highest projected chromium removal.

Table 2 shows the experimental design, which includes four parameters with three levels and 3^4 full factorial methods. There will be 81 experimental runs combining upper, middle, and lower limits. The lower (− 1), middle (0), and upper (+ 1) values of the variables were combined in these adsorption trials at random. The optimization approach of a design expert was used to set the number of experiments to 25. Finally, Eqs. 5 and 6 were used to compute the adsorption removal efficiency of the ferrite–biochar composite. The adsorption capacity of the adsorbent (q_e) was calculated based on Eq. 6 (Bedada et al. 2020; Fito et al. 2020b; Moges et al. 2022).

$$R(\%) = \left(\frac{C_i - C_f}{C_i}\right) * 100 \tag{5}$$

$$q_e = \left(\frac{C_o - C_e}{m}\right) * V \tag{6}$$

where R is the Cr(VI) removal percentage, C_i is the initial Cr(VI) concentration (mg/L), C_o (mg/L) is the initial Cr(VI) concentration, V (L) is the volume of the solution, m (mg) is the mass of the adsorbent utilized, C_e (mg/L) is the equilibrium Cr(VI) concentration, and C_f is the final Cr(VI) concentration (mg/L) after the treatment.

Table 2 Experimental design of adsorption of Cr(VI) under four factors with three factors

Variables	Low (− 1)	Middle (0)	High (+ 1)
pH	3	6	9
Time (min)	30	60	90
Adsorbent dose (mg/100 mL)	20	60	100
Initial Cr(VI) concentration (mg/L)	40ss	70	100

Adsorption isotherms

Adsorption isotherms were determined using an adsorbent dose of 100 mg/100 mL, a contact time of 90 min, a pH of 3 solutions, and solely varying the initial chromium concentrations of 40, 60, 80, and 100 mg/L. Adsorption isotherms were established to determine the relationship between the amounts of chromium adsorbed at equilibrium and the amount of adsorbent utilized per unit mass. This model was used to check whether the surface of the adsorbent is heterogeneous or homogenous. The Langmuir and Freundlich models are the two most extensively used isotherm models in water and wastewater treatment. Equation 7 was generally used for the Langmuir isotherm and the linearized form of the Langmuir model which is depicted in Eq. 8 (Bedada et al. 2020; Fito et al. 2020b; Moges et al. 2022).

$$qe = \frac{K_L q_{\max} C_e}{1 + KLCe} \tag{7}$$

$$\frac{1}{qe} = \frac{1}{q_{\max}} + \frac{1}{K_L q_{\max} C_e} \tag{8}$$

where K_L (L/mg) refers to the Langmuir constant related to the free energy of adsorption, q_{max} (mg/g) is the maximum adsorption capacity of the materials. Furthermore, Eq. 9 (RL) depicts the dimensionless separation factor constant. This factor is used to estimate Langmuir's isothermal feasibility.

$$RL = \frac{1}{1 + K_L C_e} \tag{9}$$

However, the RL value for favorable adsorption should be between 0 and 1; for unfavorable adsorption, the RL value should be more than 1, whereas RL values of 1 or 0 suggest linear and irreversible adsorption processes, respectively. Similarly, Eq. 10 is the linearized form of the Freundlich isotherm model.

$$\log\ qe = \log K_F + 1/n\ \log C \tag{10}$$

K_F denotes adsorption capacity (mg/g), and $1/n$ denotes an empirical parameter related to adsorption intensity, with a value between 0 and 1 denoting favorable conditions. Moreover, a value of $1/n$ indicates the adsorption process to be cooperative if > 1, independent of concentration if is equal to 1, and normal if < 1 (Fito et al. 2020b; Moges et al. 2022). Temkin adsorption isotherm model is one of the adsorption isotherm models used to estimate the interaction of the adsorbent and adsorbate on adsorption. This isotherm model assumes that there is a linear reduction of the heat of adsorption instead of logarithmic. Furthermore, this adsorption isotherm model is used to determine whether the nature of the adsorption is chemical, physical, or both (Rajahmundry et al. 2021). The linear form of the Temkin equation is shown by Equation 11:

$$q_e = \frac{RT}{bT} \ln K_T + \frac{RT}{bT} \ln Ce \tag{11}$$

where K_T is the equilibrium binding constant (L/mg), b_T is the Temkin heat of adsorption constant, R is the universal gas constant (8.314 J/Kmol), and T (K) is the system temperature.

Adsorbent regeneration and reusability

Various techniques are available to regenerate the exhausted adsorbent, but the solvent desorption method is the most preferred option due to its economical and effective regeneration process. However, some environmental issues need to be addressed as part of the process. Adsorbents have been found to lose their absorptive activity and generate some solid waste after repeated cycles of reusability (Patel 2021). The reusability of biochar ferrite was investigated using the chemical regeneration method. In this process, pollutant-loaded material (0.1 g) in 100 mL of NaOH (0.1 M) was shaken at 80 rpm for 2 h at room temperature. After a significant desorption process, the solution was filtered using Whatman filter paper and oven dried. The regenerated adsorbent was examined for a magnetic property before it was utilized for another cycle of adsorption. The magnetic property of the regenerated adsorbent was examined using an external magnetic field. The desorbed material was repeatedly used for up to five cycles of adsorption–desorption to check the reusability potential of the adsorbent (Santhosh et al. 2020).

Result and discussion

Batu tannery wastewater characterization

As indicated in Table 3, the results of the physicochemical properties of the effluent from the Batu tannery were presented as means plus standard deviations. The effluent was determined to have a mean temperature of 21.40 ± 0.62 °C. This temperature was far lower than 40 °C which is the limit set for Ethiopian tannery effluent. As a result, the effluent can be safely discharged into the environment, particularly into water bodies even though the high temperature of industrial effluent accelerates reaction rates which have an impact on ecosystems. Particularly, the temperature of this effluent does not affect biochemical or physicochemical processes in water bodies (Moges et al. 2022). The electrical conductivity of the wastewater sample is an important parameter that refers to the ability of wastewater to conduct electric current (Tsigoida and Argyrokastritis 2020). It helps to determine the salinity, ionic strength, and major solute concentration

Table 3 Characterization of Batu tannery wastewater

Parameter	Values
pH	4.43 ± 0.21
EC (mS/cm)	27.73 ± 1.20
Temperature (°C)	21.40 ± 0.62
BOD_5(mg/L)	300.97 ± 2.22
COD (mg/L)	1992.67 ± 7.21
TS (mg/L)	318.07 ± 4.27
SO_4^{2-}(mg/L)	119.17 ± 4.10
PO_4^{3-}(mg/L)	21.53 ± 0.81
Cr^{6+}(mg/L)	85.13 ± 1.22

of water or wastewater (Chowdhury et al. 2015; Fito and Van Hulle 2021). Moreover, the electrical conductivity of wastewater is affected by the properties of substrate materials, the temperature of the environment, and the concentration of the pollutants found in the wastewater. The electrical conductivity of Batu tannery wastewater was found to be 27.73 ± 1.20 mS/cm. This value is far above the 12 mS/cm standard limit set by the WHO, indicating an unfavorable environment for the aquatic biota (WHO 2012). The significant amount of chromium salt added during the tanning process is accountable for this high value of electrical conductivity (Jahan et al. 2014). Throughout the study, the average pH of the effluent was 4.43 ± 0.21. This is an extremely acidic rating that falls outside of the maximum allowable discharge limits. The pH of effluent should be in the range of 6–9, according to Ethiopian industrial acceptable limits. This acidic feature influences the metabolic reactions of a living organism with physicochemical and biochemical processes. Acidic media also may increase the solubility of organic and inorganic substances, particularly heavy metals, in the environment. Water bodies and soils are the two segments of environment that receive untreated wastewater, which are most likely to be impacted by such pollution. As a result, effluent treatment, such as chemical neutralization, is required before the effluent can be released into the environment (Fito et al. 2019a; Moges et al. 2022).

COD and BOD_5 are the two major parameters used to describe the presence of organic matter in wastewater. In Batu tannery effluent, the average values of BOD_5 and COD were 300.97 ± 2.22 mg/L and 1992.67 ± 7.21 mg/L, respectively. These BOD_5 and COD levels were higher than the tannery's effluent discharge limits of 60 mg/L and 250 mg/L, respectively. Organic matter levels in the wastewater were extremely high, posing a serious threat to aquatic bodies and agricultural fields. This high organic matter concentration could be an underutilized resource for biogas production and environmental health (Moges et al. 2022). Moreover, the biodegradability index, which is a ratio of BOD_5 to COD of Batu tannery effluent, was determined to be 0.15, indicating poor biodegradability. Therefore, it is evident that another treatment technology has to be sought rather than biological treatment (Fito et al. 2017). Similarly, the effluent contains 318.074 ± 0.27 mg/L of total solid matter, which was far too high to discharge into the environment before treatment. This high value is due to the presence of filterable and non-filterable particulate matter in the wastewater samples. This particle matter can cause turbidity and reduce transparency in water bodies, disturbing natural aquatic ecosystems. Additionally, high total solid concentrations have a considerable impact on dissolved oxygen depletion. The fundamental reason for interrupting interactions between living things and metabolic activity in water bodies is a lack of dissolved oxygen, putting aquatic life in peril. The physicochemical and biological qualities of soil and water bodies, in general, can be affected by such high total solid matter concentrations.

Sulfates and phosphates are among the other chemicals utilized in the tanning process. Sulfates and phosphates in Batu tannery wastewater were found to have average levels of 119.17 ± 4.10 and 21.53 ± 0.81 mg/L, respectively. Salts utilized in tannery processes are proven to contain phosphate and sulfate ions. These high ion concentrations can have negative consequences for water systems and soils. As a result, treatment intervention is critical for environmental and public health protection (Moges et al. 2022). Chromium is the most common consumable chemical in the tanning process and an abundant pollutant in wastewater. Throughout the study period, the average chromium content was 85.13 ± 1.22 mg/L. The environment can be seriously harmed by high levels of chromium. This pollutant is a highly soluble and migratory ion in water and a highly toxic substance in the environment. Diseases such as kidney dysfunction, skin irritation, hepatitis, lung disease, pulmonary congestion, vomiting edema, and liver damage can all be caused by this chromium content (Bedada et al. 2020). Cr(VI) is a major pollutant in both surface and groundwater, where it can spread widely due to its high ionic mobility. This high chromium concentration in tannery wastewater is beyond the maximum allowed discharging limit of tannery effluent set by EPAs of many countries. Cr(VI) concentrations in drinking water, surface water, and industrial effluent discharge are set at 0.1, 0.1, and 0.25 mg/L, respectively (Parlayici et al. 2015; Huang et al. 2018; Aigbe and Osibote 2020; Bedada et al. 2020; Moges et al. 2022) Moreover, the maximum allowable Cr(VI) concentration in drinking water has been set at 0.05 mg/L by the World Health Organization.

Adsorbent characterization

Proximate analysis

The percentage results of the proximate analysis of biochar–magnetite composite were reported in terms of

Table 4 Proximate analysis of magnetite–biochar composite derived from parthenium hysterophorus

Proximate analysis	Value (%)
Moisture content	5.2
Ash content	13.3
Volatile matter	19.4
Fixed carbon	62.1

moisture content of 5.20%, volatile matter of 19.4%, ash content of 13.30%, and fixed carbon of 62.1%, as shown in Table 4. Fixed carbon and ash content are the most essential criteria of the proximate analysis to determine the quality of the adsorbent materials. A suitable precursor material should typically contain a high percentage of fixed carbon and a very small amount of ash. In the proximate analysis, fixed carbon refers to non-volatile carbon, whereas ash content refers to undesired inorganic oxides that can be observed during biochar magnetic preparation (Fito et al., 2020c). Normally, a high percentage of volatile matter positively affects the development of the micropore structure during the pyrolysis process. However, it decreases biochar yield. Many laboratory-scale-produced ferrite–biochar composites have very low fixed carbon content. For instance, the fixed carbon of wheat straw-based magnetic biochar is 48.7% (Wurzer and Mašek 2021), magnetic dry wood biochar is 33.8% (Sewu et al. 2020), and cotton straw-derived magnetic biochar is 25.9% (Shan et al. 2019). However, the fixed carbon content of currently produced magnetic biochar derived from parthenium hysterophorus is slightly greater than that of its pristine activated carbon, as reported by Fito et al., 2020c, whereas its ash content is less. In general, the outcome of the proximate analysis is not solely determined by the precursor material, because varying degrees of dehydration, decomposition, and elimination reactions are expected at different temperatures. These results of the proximate analysis are greatly influenced by carbonization processes (Fito et al., 2020c). Finally, magnetic biochar derived from parthenium hysterophorus thus holds promise as a more sustainable alternative to coal-derived magnetic-activated carbons or biochar.

pH point of zero charge

When the pH of the adsorbent equals its pHpzc, there is an equal number of positively and negatively charged surface functions Fig. 5. The surface is positively charged below this value and negatively charged above this value. Basically, it is easier to adsorb a cation on negatively charged surfaces and an anion on a positively charged surface (Rodr et al. 2020; Pashai et al. 2016; Tang et al. 2019; Rusmirovic and Milo 2021). The pH point of zero charges of the magnetite–biochar composite derived from parthenium hysterophorus was found to be 6.8. A nearly similar

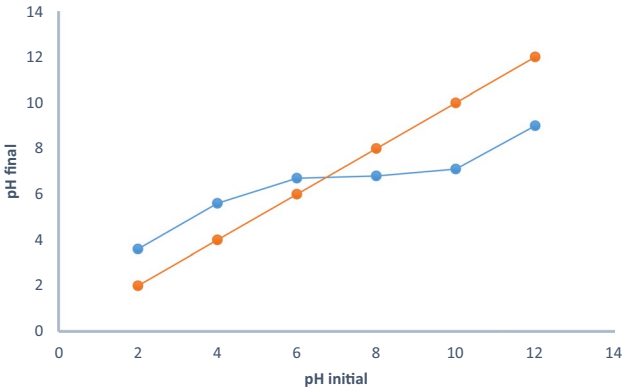

Fig. 5 The pH point of zero charge

result was reported by Ud et al. 2021. The pHpzc of this biochar-magnetite composite was reduced as a result of the magnetizing process. Moreover, the decrease in point of zero charge could also be due to the oxidation of carbon surfaces at the initial stage of the magnetizing process (Navarathna et al., 2019a, 2019b; Imran et al. 2020a; Ud et al. 2021).

BET analysis

The BET-specific surface area of the biochar–magnetite composite derived from parthenium hysterophorus was 237.4 m^2/g. The type of N_2-adsorption desorption isotherm observed in the study was type II adsorption which implies the adsorbent was normal and macroporous of a wide range of pore sizes. This adsorption process is of unrestricted monolayer-multilayer nature even though more of the monolayer is the most dominant that manifested with adsorption isotherm models. Usually, the bi-layer and tri-layers will be formed one after the other. The specific surface area of this magnetic biochar is approximately 4.2 times siltstone and its composites with biochar and magnetite nanoparticles (Imran et al. 2020a), 16.74 times watermelon rinds-based biochar–magnetite composite (Li et al. 2020a), 1.08 times mixed wood chips biochar/magnetite composite (Han et al. 2015), 6.21 times magnetic Kans grass biochar (Baig et al. 2014), and 0.82 times GO-Fe_3O_4 nanocomposites (Moges et al. 2022). This surface area is, therefore, greater than that of many magnetic biochar adsorbents reviewed in this paper, allowing for the adsorption of different pollutants from wastewater or aqueous solutions. Normally, increasing surface area leads to an increased number of active sites available for adsorption, thereby increasing adsorption capacity. However, there were no evident increasing or decreasing patterns seen in the surface area of the biochar–spinel ferrite composite (Fito et al. 2022).

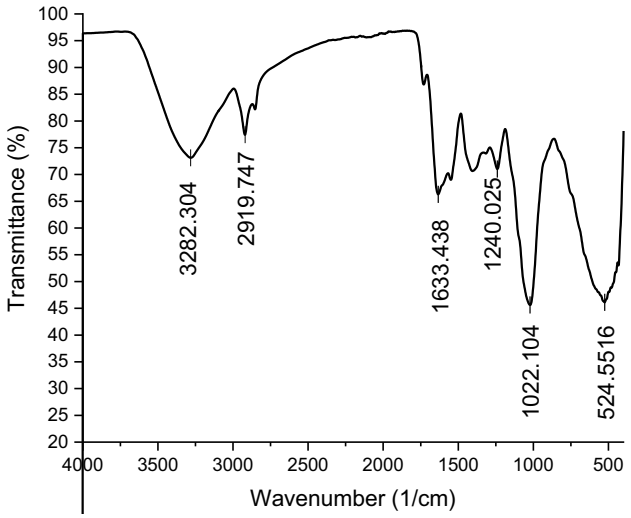

Fig. 6 FTIR patterns for biochar–magnetite composite

FTIR analysis

The surface functional groups of biochar–magnetite composite derived from parthenium hysterophorus were identified using FTIR spectra. Six distinct peaks were observed as shown in Fig. 6. Therefore, the peaks of 3296.49 cm^{-1}, 2920.5 cm^{-1}, 1608.7 cm^{-1}, 1317.14 cm^{-1}, 1147.09 cm^{-1}, and 1010.47 cm^{-1} are the prominent peaks. The presence of several peaks in the FTIR spectrum demonstrates the adsorbent's complex structure. The presence of free and intermolecular bound hydroxyl groups is shown by the signal at 3282 cm^{-1}. It is also linked to the hydrogen-bonded O–H group's valence vibration. The C–H stretching in the ($–CH_2$) and ($–CH_3$) groups resulted in the 2919 cm^{-1} shoulder band. The symmetric (NH_3^+) stretching frequency or the carbon–oxygen bonds in the ketene groups correspond to the large band at 1633 cm^{-1}. Ketones, aldehydes, lactones, or carboxyl groups' C = O stretching vibrations are allocated into a very small peak at about 1240 cm^{-1}. The presence of C–H, –C = C– and aromatic (C = C) groups is indicated by the band at 1147 cm^{-1}. The peak at 1010 cm^{-1} denotes the solitary C–O bond as well as the CH bending vibration of $C–H_2$ and $C–H_3$. Finally, 524 cm^{-1} reveals the stretch of Fe_3O_4 (Liang et al. 2020; Ud et al. 2021), confirming magnetite impregnation on the surface of biochar. The adsorbent peaks revealed the presence of functional groups on the surface of the adsorbent that can react with the various adsorbates in the solution (Bedada et al. 2020; Fito and Van Hulle 2021).

SEM analysis

The surface morphology of the biochar–magnetite composite derived from a parthenium hysterophorus sample was examined using scanning electron microscopy (SEM) before it was used for adsorption. The image of the SEM analysis was indicated in Fig. 7. In this study, the surface of the composite material was magnified 3000 times, which clearly showed the different pore sizes and their distributions. The composite adsorbent was found to have highly uneven surfaces that are highly heterogeneous and filled with cavities, holes, ruptures, voids, fractures, fissures, nooks, and crannies. These characteristics serve as the places that enhance surface sorption. Moreover, the high temperature during carbonization and calcination results in escaping of volatile matter inside the microstructure of the particles. This process creates voids on the surface of the adsorbent that eventually become pores. Generally, heterogeneous surfaces of the adsorbent can create a conducive condition to adsorb various pollutants from water and wastewater (Ighalo and Adeniyi 2020).

XRD analysis

The crystalline structure of the magnetite–biochar composite was investigated using the X-ray diffraction technique. Figure 8 depicts the findings of the XRD analysis. The materials had crystalline characteristics at 2θ of 30.15, 35.51, 43.16, 53.32, and 57.08 with corresponding peaks of (220), (311), 400), (422), and (511). The dominant peak pattern observed for the composite materials was primarily due to the magnetite component of the adsorbent. Because of its amorphous nature, the peaks of parthenium hysterophorus-derived biochar are not expected to emerge in the XRD pattern. These outcomes are quite similar to those observed by Zahedifar et al. 2021, in which peaks of magnetic biochar material emerged at 30.5°, 35.9°, 43.5°, 53.9°, 57.4°, and 63.0°.

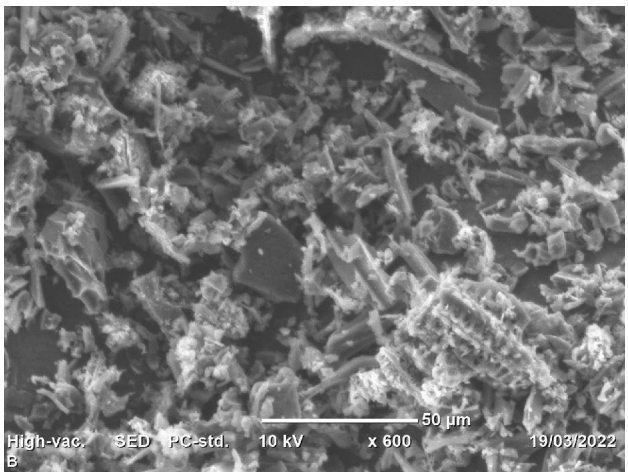

Fig. 7 SEM surface morphology of the biochar–magnetite composite

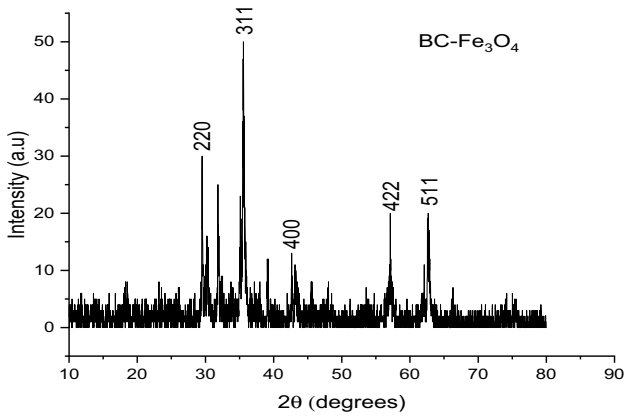

Fig. 8 XRD peaks of biochar–magnetite composite adsorbent

Batch adsorption of Cr(VI)

The Box–Behnken technique of the response surface methodology experiment was used to remove Cr(VI) from synthetic tannery effluent, and the adsorption treatment outcomes are shown in Table 5. The performance of this technology ranged from 17.3 to 91.8%. Under this optimization process of the adsorption, 91.8% was the maximum chromium removal from synthetic tannery wastewater at the optimum conditions of adsorbent dose of 100 mg/100 mL, pH of 3, initial Cr(VI) concentration of 40 mg/L, and contact time of 90 min. The minimum Cr(VI) removal of 17.3% was observed at specific experimental conditions of initial Cr(VI) concentration of 100 mg/L, 20 mg/100 mL of adsorbent dose, pH of 9, and contact time of 30 min. This experimental result is superior compared to that of pristine parthenium hysterophorus activated carbon which was applied for chromium removal from tannery wastewater which was recorded at pH of 2, Cr(VI) concentration of 100 mg/L, adsorbent dosage of 10 g/110 mL, and contact time of 90 min) (Bedada et al. 2020). Even though the magnetite nanoparticle did not show significant improvement in the adsorption performance, it has a huge advantage in helping spent adsorbent separation after the treatment. Hence, magnetite impregnation has improved the wastewater management part of the adsorption of biochar. Changing the pH of the treatment from higher to lower has resulted in an adsorption performance of 41.1% and 31.3% with concentration, adsorbent dosage, and contact time kept at 100 mg/L, 20 mg/100 mL, and 30 min, respectively. The

Table 5 Results of batch adsorption experiments

No. of run	pH	Initial Cr(VI) conc. (mg/L)	Dose (mg/100 mL)	Contact time (min)	Removal (%)	Final Cr(VI) conc. (mg/L)
1	9	100	20	30	17.3	82.7
2	3	70	20	30	43.8	39.29
3	6	40	20	30	48.0	20.8
4	9	40	20	30	44.3	22.3
5	6	100	60	30	55.2	44.8
6	3	70	100	30	73.9	20.8
7	3	100	20	30	41.1	58.9
8	6	100	20	30	31.3	68.7
9	3	100	60	30	64.9	35.1
10	6	40	60	30	58.8	16.5
11	9	40	100	60	73.5	10.6
12	3	40	60	60	88.1	4.7
13	6	100	20	60	43.8	56.2
14	3	100	20	60	43.7	56.3
15	3	70	20	60	44.1	39.1
16	9	100	100	60	65.0	35.0
17	6	70	20	90	43.9	39.3
18	3	40	100	90	91.8	3.3
19	6	70	60	90	56.2	30.7
20	6	40	60	90	76.8	9.3
21	6	40	100	90	89.0	4.4
22	3	40	20	90	54.3	18.3
23	3	70	100	90	90.8	6.4
24	6	100	100	90	69.3	30.7
25	3	70	60	90	79.1	14.6

adsorption performance under the influence of the pH at the constant values of other factors was insignificant. Essentially, the interaction effect is more important than the change in adsorption parameters when it comes to increasing or increasing adsorption treatment. The final Cr(VI) content in the effluent was above the standard in many cases of adsorption treatment, although it was able to decrease the Cr(VI) concentration to 3.3 mg/L, 4.4 mg/L, and 4.7 mg/L at particular treatment levels.

The concentration of Cr(VI) in real wastewater was determined to be 85.13 mg/L. In synthetic wastewater, the maximum Cr(VI) concentration was 100 mg/L which was approximately the same as in real wastewater. The removal of Cr(VI) at the high concentration was found to be 75.9% which was equivalent to the remediation (81.8%) from real wastewater. Reducing contact time from 90 to 30 min, raising the initial Cr(VI) concentration from 40 to 100 mg/L, lowering the adsorbent dose from 100 to 20 mg, and increasing pH from 3 to 9 resulted in the reduction of adsorption performance from 91.8 to 79.4%, 81.8%, 61.6%, and 89.4%, respectively. Hence, the change in adsorbent dosage significantly affected the adsorption performance. Similarly, increasing the initial Cr(VI) concentration from 40 to 100 mg/L while maintaining the other parameters constant (pH 6, contact time of 90 min, and adsorbent dose of 60 mg/100 mL) reduced overall Cr(VI) removal efficiency. Changing the pH value from 4 to 9 resulted in a continual decrease in adsorption performance. However, changing the contact time from 30 to 90 min resulted in a minor improvement in adsorption performance under the same experimental conditions. The results show that the performance of the biochar–magnetite composite treatment technology was effective and efficient. Compared to the treatment performance reported by other research findings, the chromium removal capacity of this technology is superior. For instance, the removal of chromium using quinoa–biochar composite was 77.4 mg/g (Imran et al. 2020b), siltstone–nano magnetite–biochar composite was 35.6 (Ud et al. 2021), a magnetite snail shell was 58.9 mg/g (Hoang et al. 2020), tires waste-derived magnetic-activated carbon was 49.3 mg/g (Ahmad et al. 2021), and graphene biochar–iron oxide composites was 48.1 mg/g (Zou et al. 2021).

Compared to many locally prepared magnetite activated carbons, the magnetite adsorbent of this study showed superior performances. The detailed preparation of the adsorbent, specific surface areas, and adsorption performances are presented in Table 6 However, many experiments were applied for the removal of Cr from aquatic solution and a few were focused on Cr removal from real wastewater. Moreover, these studies suffer from excessive use of adsorbents for removal of small amounts of Cr. Hence, the current study serves as an alternative method of Cr adsorption from wastewater and aqueous environment using the small adsorbent dose, which makes the current study economical.

Interaction effects on Cr(VI) removal

The adsorption experiments of the study were designed by response surface methodology whereas the response variability was predicted using the quadratic model. The impacts of the main and interaction effects on adsorption were investigated using ANOVA. Terms of actual factors were used

Table 6 Chromium adsorption using different biomass-based magnetic biochar

No	Adsorbent	Synthesis method	Surface area m^2/g	Removal (%, mg/g)	Reference
1	Fe_3O_4–biochar/cellulose	pyrolysis	236.0	19.8	(Zhou et al. 2022)
2	Fe_3O_4–biochar/C. oleifera	pyrolysis	12.2	107.0	(Sun et al., 2021)
3	Fe_3O_4–biochar/bagasse	microwave	17.8	55.0	(Bai et al., 2021)
4	Fe_3O_4–biochar/bambo	pyrolysis	243.4	48.0	(Wang et al., 2017)
5	Fe_3O_4–biochar/ raspberry	Pyrolysis	163.0	16.3	(Dobrzyńska et al., 2022)
6	Fe_3O_4–biochar/N.Sativa	hydrothermal	–	13.0	(Thabede et al., 2021)
7	Fe_3O_4–biochar/rice husk	Microwave	76.9	84.3%	(Zhong et al., 2018)
8	Fe_3O_4–biochar/quinoa	Coprecipitation	–	77.4	(Imran et al. 2020a, b)
9	Fe_3O_4–biochar/ bagasse	Pyrolysis	26.9	71.0	(Yunqiang Yi et al., 2020)
10	Fe_3O_4—biochar–hickory	Ball milling	241.0	50.6	(Zou et al. 2021)
11	Fe_3O_4–biochar/cotton silk	Microwave	129.2	67.4	(Duan et al., 2017)
12	Fe_3O_4–biochar/bamboo	Pyrolysis	317.8	19	(Wang et al., 2017)
13	Fe_3O_4–biochar/odorata	Co-precipitation	35.7	52.8%	(Nnadozie & Ajibade, 2020)
14	Fe_3O_4_biochar/reed	Microwave	154.8	9.92	(Song et al., 2020)
15	Fe_3O_4–biochar/reed straw	Pyrolysis	1.1	40.0	(Qin et al., 2020)
16	Fe_3O_4–biochar/P. Hysterophorus	Co-precipitation	237.4	69.3	Current study

to make predictions about the response for given levels of each factor. The ANOVA results of the study are presented in Table 7. The four factors with a three-level matrix were generated by Box–Behnken design for adsorption of Cr(VI) as the response variable. Based on this, the response surface quadratic model analyses were performed and many significant terms of the main factors were observed, whereas the second-order terms were almost insignificant. The analysis also indicated that the most influential factor in the adsorption process was the adsorbent dose, whereas the least influential factor was contact time. On the contrary, the interaction between the contact time was the only significant term among the second-order quadratic levels. Normally, only those significant terms have real impacts on Cr(VI) removal performances.

Adsorbent dosage and pH

The effect of interactions on the response variable was evaluated using the analysis of response surface methodology. In this approach, the difference between projected and actual Cr(VI) removal was compared. Based on the adsorption performance of magnetic biochar, the reduction of Cr(VI) ranged from roughly 18 to 92% in this study. The distribution of the actual values was a nearly perfect fit with the experimental data, as shown by the linear plot projected against real data. The ANOVA test indicated that the data were well fitting. Response surface plots and contour maps are widely used to depict the relationship between the response variable and the interaction of the two factors in a pictorial manner. Figure 9 shows a 3D plot of response surface methods that were used to statistically correlate the interaction effect to the response variable. The expected Cr(VI) removal efficiency was shown to be a result of the interaction effects. The interaction effect of the adsorbent dose and pH had a negative effect on the efficiency of Cr(VI) removal. At an initial chromium concentration of 70 mg/L and a contact time of 90 min, this projected removal efficiency ranged from 35 to 85%. At the interaction effect between an adsorbent dose of 100 mg and a pH of 3.0, the maximum Cr(VI) removal efficiency of 85% was recorded. In general, it is evident from the graphical representation that chromium removal efficiency increased as the adsorbent dosage was increased and the pH of the solution was decreased. A similar result was reported by (Narzari et al. 2021) where the interaction effects of adsorbent dosage and pH of the solution were found to have a negative effect on chromium Cr(VI) removal using Lantana Camara-derived magnetic biochar.

Cr(VI) concentration and adsorbent dosage

The interaction effect of adsorbent dosage and initial chromium concentration on the chromium removal efficiency is shown in Fig. 10. It was observed that an increase in initial chromium concentration from 40 to 70 mg/L decreased the chromium removal efficiency from 49.7 to 42.8% when the adsorbent dosage was kept at 20 mg/100 mL. Similarly, keeping the initial chromium concentration at 40 mg/L, an increase in the adsorbent dosage from 20 mg/100 mL to 60 mg/100 mL increased the chromium removal efficiency from 49.8 to 67.1%. Normally, increasing initial chromium

Table 7 Quadric model – ANOVA results for the response surface methodology optimization

Source	Sum of squares	df	Mean square	*F* value	*p* value	Significant
Model	9175.30	14	655.38	19.50	< 0.0001	**
A-pH	538.19	1	538.19	16.01	0.0025	**
B-Cr(VI) conc	695.26	1	695.26	20.68	0.0011	**
C-Adsorbent dosage	2012.32	1	2012.32	59.87	< 0.0001	**
D-contact time	109.15	1	109.15	3.25	0.1017	*
AB	61.79	1	61.79	1.84	0.2050	*
AC	95.85	1	95.85	2.85	0.1222	*
AD	2.90	1	2.90	0.0864	0.7748	*
BC	85.78	1	85.78	2.55	0.1412	*
BD	45.86	1	45.86	1.36	0.2699	*
CD	69.82	1	69.82	2.08	0.1801	*
A^2	1.92	1	1.92	0.0571	0.8160	*
B^2	16.37	1	16.37	0.4871	0.5012	*
C^2	135.11	1	135.11	4.02	0.0728	*
D^2	167.82	1	167.82	4.99	0.0495	**
Residual	336.12	10	33.61			
Cor total	9511.42	24				

**significant terms and *insignificant terms

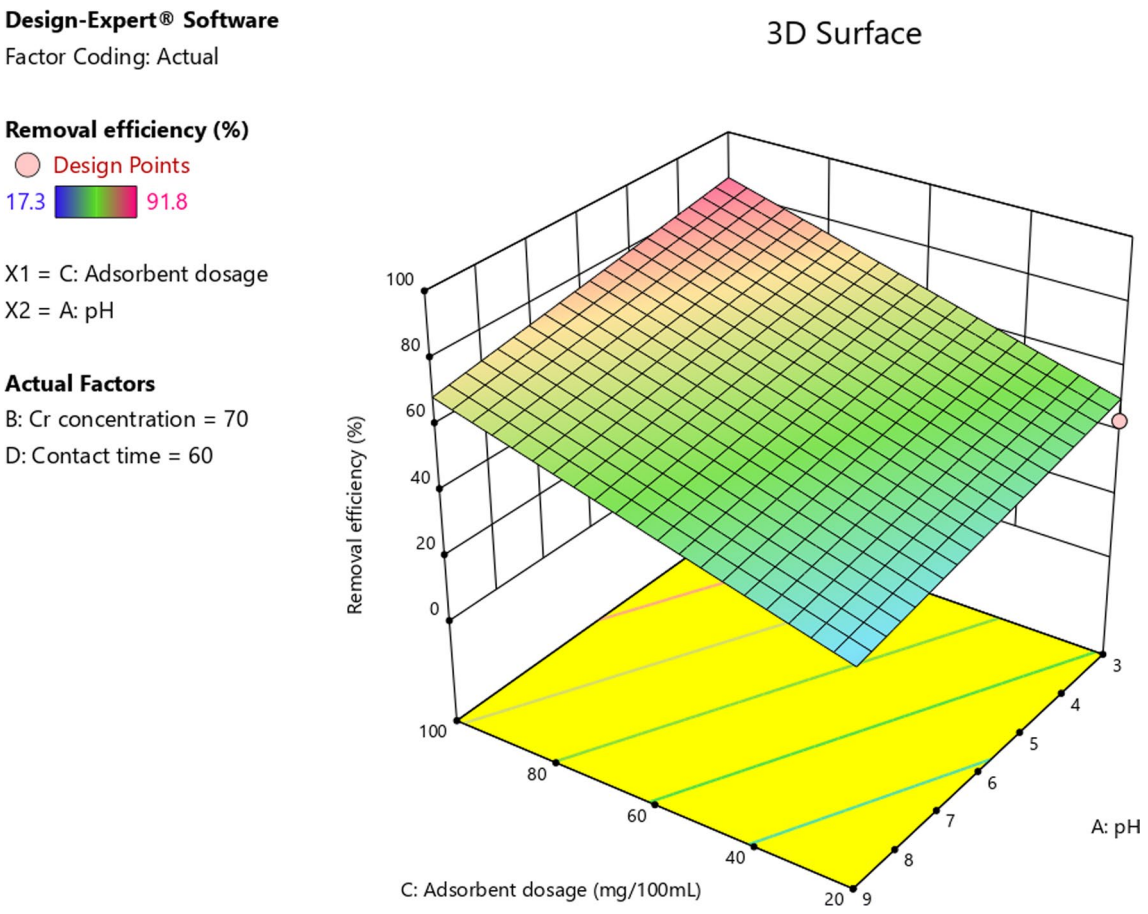

Fig. 9 The interaction effect of adsorbent dosage and pH on removal efficiency

concentration while keeping the other parameters decreases the overall removal efficiency, whereas increasing adsorbent dosage increases the removal efficiency. Moreover, a 3D graph sketched using initial chromium concentration and adsorbent dosage shows that the interaction of adsorbent dosage and initial chromium concentration positively influenced chromium removal efficiency. Finally, the interaction effects of the initial chromium concentration and adsorbent dosage on the removal of Cr(VI) can be supported by the results reported by (Narzari et al. 2021; Moges et al. 2022).

Initial Cr(VI) concentration and contact time

To estimate the combinations of the independent factors on Cr(VI) removal, three-dimensional response surface plots were used. The influence of contact time and initial chromium content on adsorption was studied, and the pattern of interaction is shown in Fig. 11. The response surface plots for Cr(VI) removal were used to further develop this notion. The interaction effect was found to have an unfavorable influence on the removal efficiency of Cr(VI). Separately, the initial chromium concentration negatively affects Cr(VI) removal, while contact time had a positive impact. The maximum Cr(VI) removal efficiency of 70% was recorded at the interaction effect between the interaction of contact time of 90 min and an initial chromium concentration of 40 mg/L, as shown in the 3D figure. The findings showed that as contact time increases at a fixed initial Cr(VI) concentration, percentage removal increases. While the contact time decreases as the initial chromium concentration increases and removal efficiency decreases. This result is in good agreement with the finding obtained by Moges et al. 2022, where Fe_3O_4–GO was used to remove Cr(VI).

Initial chromium concentration and pH

Figure 12 shows the combined effect of pH and initial chromium concentration on Cr(VI) removal effectiveness at a constant adsorbent dosage (60 mg/100 mL) and contact time (60 min). The interaction effect was found to have a negative impact on the removal efficiency of Cr(VI). It was tested with a fixed adsorbent dose of 60 mg and a contact time of 90 min. The proportion of Cr(VI) ions removed increased as the initial concentration of Cr(VI) ions and solution pH were

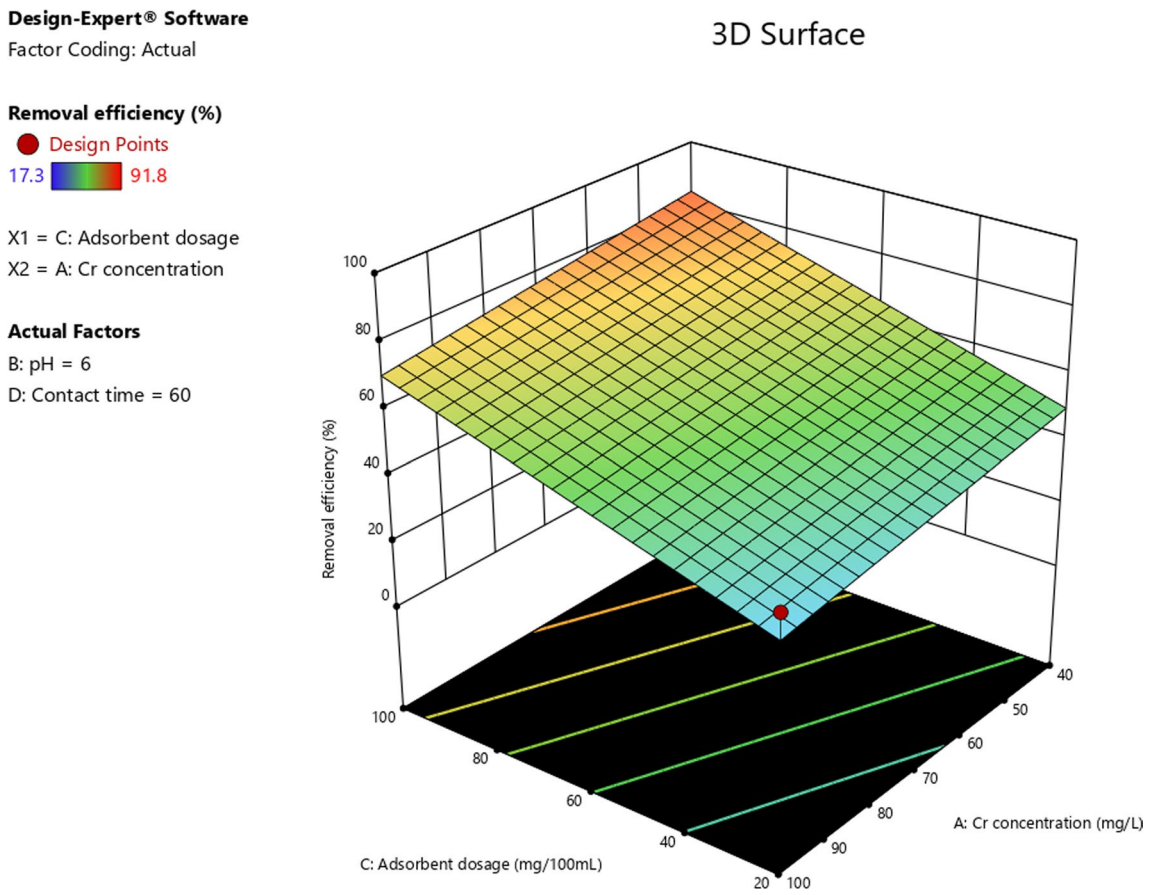

Fig. 10 The interaction effect of adsorbent dosage and Cr(VI) concentration on removal efficiency

reduced. This can be explained by the fact that all adsorbents have a finite number of active binding sites, which become saturated at a particular concentration (Moges et al. 2022). At the interaction effect of initial chromium content of 40 mg/L and a pH of 9.0, the maximum Cr(VI) removal efficiency of 75.4% was recorded. As indicated in Fig. 12, pH increases from 3.0 to 9.0, and the removal efficiency declines. The same trend with findings was reported by Narzari et al. 2021. In their study, the authors reported that the interaction effects of initial chromium concentration and pH negatively affected the removal efficiency of Cr(VI).

Adsorption isotherms

The plot of 1/Ce against $1/q_e$ was used for the analysis of the Langmuir model and the graphical representation of the Langmuir isotherm model is indicated in

Figure. 13 . The calculated values for the Langmuir adsorption capacity (q_{max}), correlation coefficient, and binding energy constant (K_L) were 400 mg/g, 0.99, and 0.031 L/mg, respectively. The Langmuir adsorption capacity of 400 mg/g shows the best performance of the composite adsorbent. Dimensionless equilibrium parameter (R_L) was calculated to know whether the process is favorable or not for the Langmuir type adsorption. The calculated R_L value found in this study was 0.45 representing a favorable adsorption process that shows the effectiveness of the interaction of the adsorbent with the Cr(VI) ion (Moges et al. 2022). Similarly, the linearized Freundlich isotherm was used and the plot of log Ce against log q_e was carried out which resulted in a regression coefficient of R^2 0.99 as shown in

Figure. 14 .The value of 1/*n* and Freundlich constant (*n)* were 0.85 and 1.183, respectively, indicating that the sorption of Cr(VI) onto the biochar magnetic sorbent is favorable. To evaluate the applicability of the Temkin isotherm model, a plot of ln*Ce* against q_e was established. The correlation coefficient of Temkin isotherm model for adsorption data fitted with experimental data was determined to be 0.95. The values for the Temkin isotherm equilibrium constant (KT) and the constant related to the heat of sorption (b) were found to be 0.6263 L/g and 47.89 J/mol, respectively. Figure 15 shows the graphical representation of the Temkin adsorption isotherm for Cr(VI) removal using the magnetite–biochar composite. Moreover, the *B* value of 47.89 J/mol (0.0115 kcal/mol), which was less than 1 kcal/mol indicates that the adsorption of Cr(VI) onto biochar–magnetite

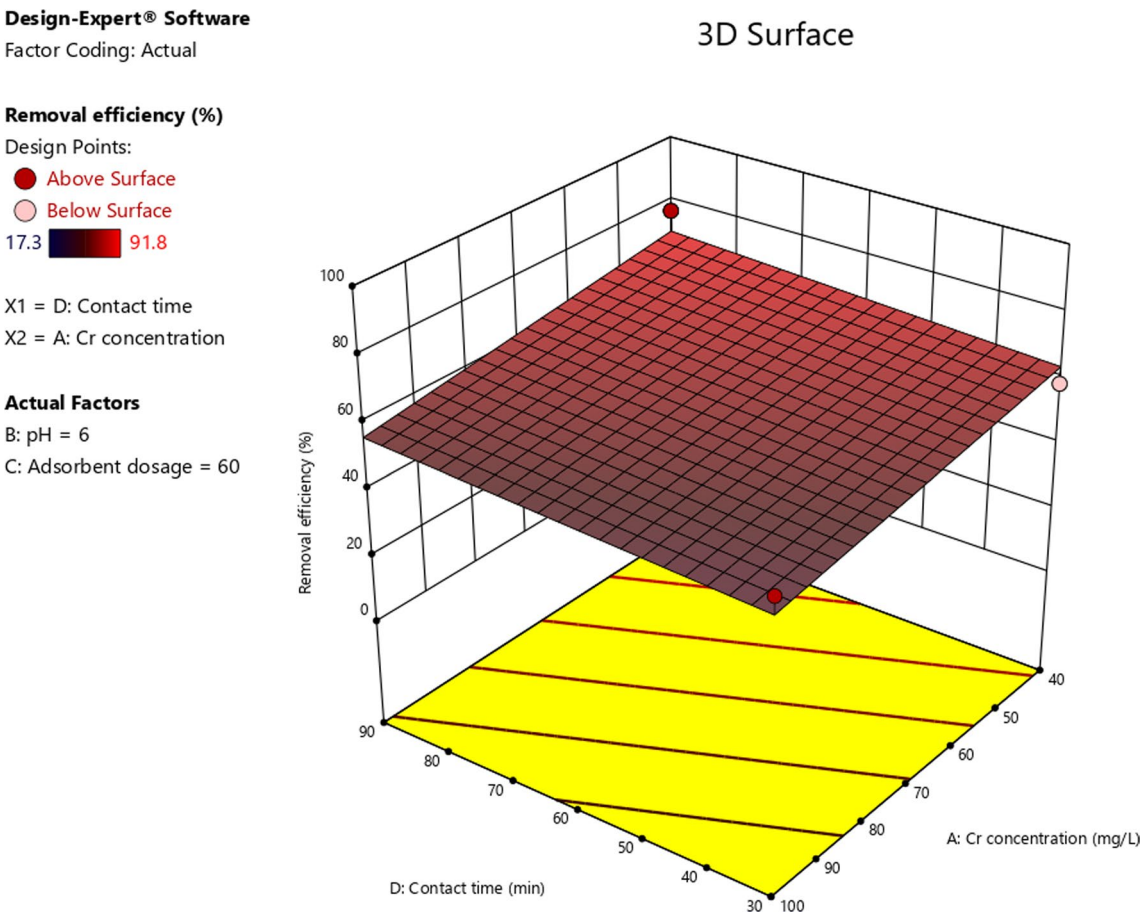

Fig. 11 The interaction effect of contact time and Cr(VI) concentration on removal efficiency

composite is more physical. Based on these results, the determined correlation coefficient shows that the adsorption of Cr(VI) more resembled the Langmuir model. This indicated that Langmuir was more explanatory. Hence, the surface of the adsorbent is homogenous and the active sites of the adsorbent are linearly distributed. Furthermore, the value of 1/*n* was found to be less than 1 which implies normal adsorption. Predicting the right adsorption mechanism is not straightforward since it is influenced by neutral molecules vs. dissociated ions, polar versus non-polar, and hydrophobicity vs. hydrophilicity (Tong et al., 2019a). The adsorption mechanism is demonstrated by the occurrence of surface precipitate, coordination formation, and the dis/appearance or shifting of the functional and crystal peaks (Du et al., 2022; Liu et al. 2022). The common adsorption mechanisms were described by hydrophobic effect, covalent bonding, coulombic interaction, π-π electron donor–acceptor, electrostatic interactions, surface complexation, ion exchange, H-bonding, π-interaction, and dipole interactions (Jemal and Thabo, 2022; Kokkinos and Mantzavinos, 2020; Ru et al., 2021; Tong et al., 2019b; Wang et al., 2018). In this study, physisorption was the dominant mechanism which can be demonstrated by van der Waals forces, hydrogen bonding, and hydrophobic interactions.

Regeneration and reusability

The adsorption efficiency of biochar–magnetite composite for Cr(VI) removal was performed five times through adsorption–desorption cycles. Figure 16 shows that the adsorption efficiency of biochar–magnetite composite was 91.8% at the initial stage and the performance at the fifth cycle was 39.2%. This shows a significant reduction in adsorption performances. The removal efficiency exhibited a continuously decreasing trend when the number of adsorption–desorption cycles increased. The reduction in the adsorption performance was probably due to the loss of the active sites associated with incomplete desorption. Furthermore, the decrease in removal capacity after successive cycles reveals the regeneration capacity of the adsorbent for further reuse of the adsorbent. Therefore, the obtained results proved that biochar–magnetite composite possessed high reusability and stability, which could give it great potential for practical application for Cr(VI) removal.

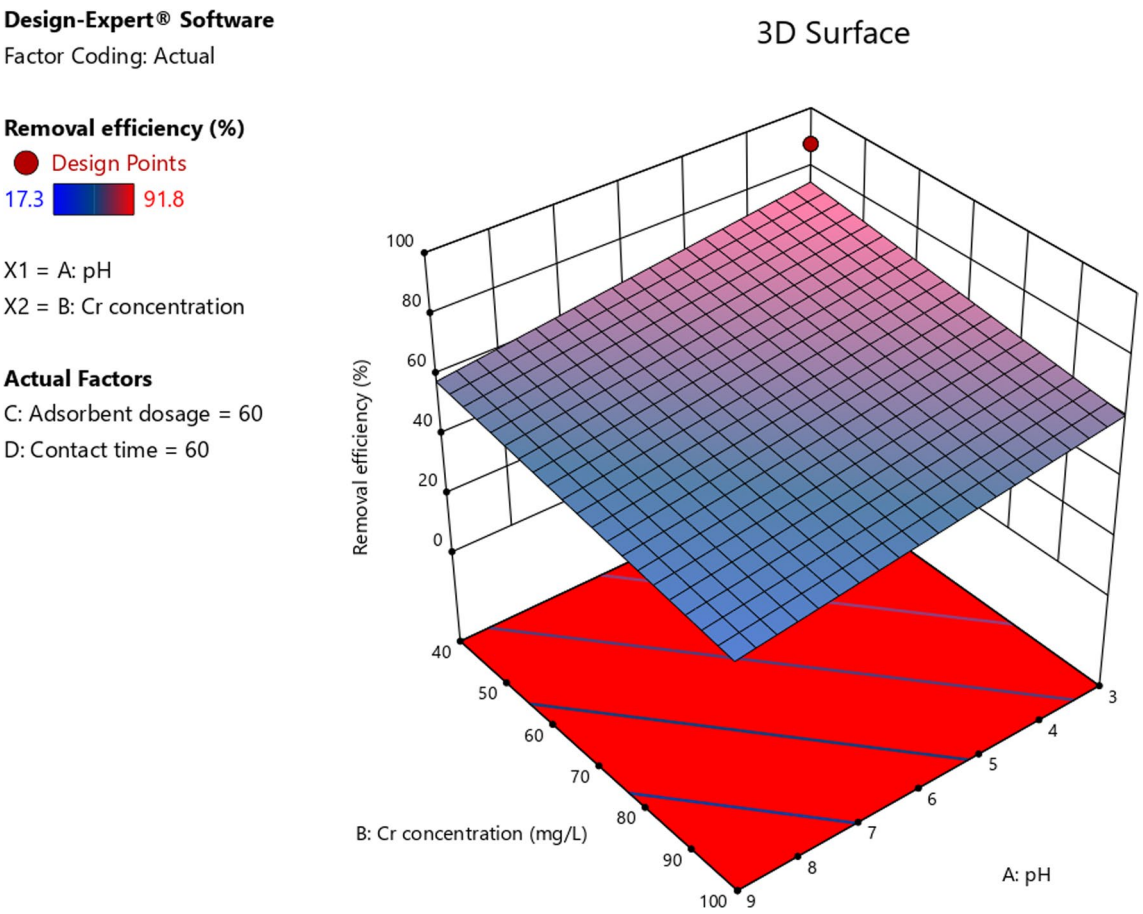

Fig. 12 The interaction effect of pH and Cr(VI) concentration on removal efficiency

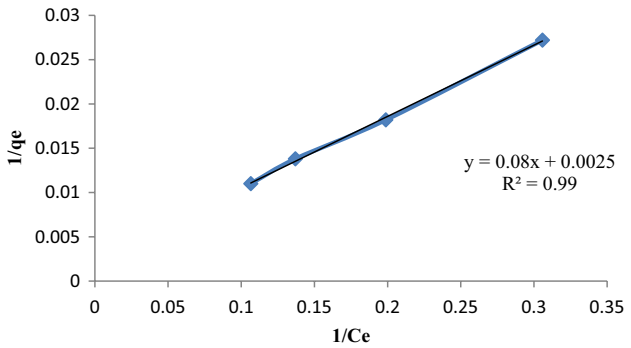

Fig. 13 Langmuir isotherms for Cr(VI) removal at the optimum point

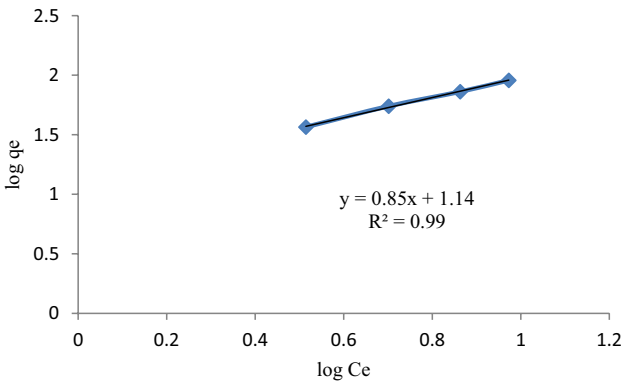

Fig. 14 Freundlich model for the removal of Cr(VI) using biochar–magnetite composite

Conclusions

The investigation of tannery wastewater was performed and Cr(VI) concentration was found to be 85.13 ± 1.22 mg/L. Adsorption treatment technology was applied for Cr(VI) removal from the tannery wastewater. Based on this approach, biochar was developed from the parthenium hysterophorus plant and modified using magnetic Fe_3O_4 which resulted in a biochar-magnetite composite adsorbent. This synthesis of composite adsorbent was successfully synthesized through the coprecipitation method. Optimization of the adsorption process was effectively carried out through response surface methodology,

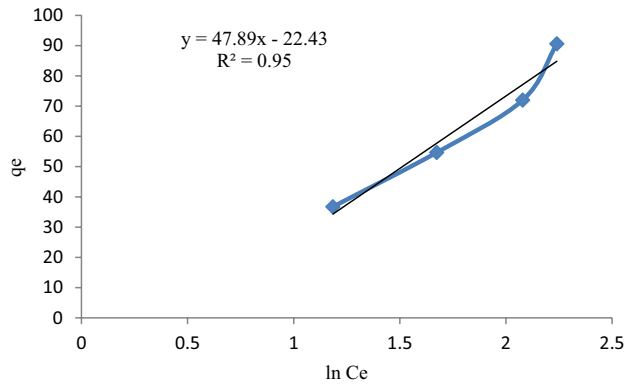

Fig. 15 Temkin isotherms model for removal of Cr(VI) by using biochar–magnetite composite

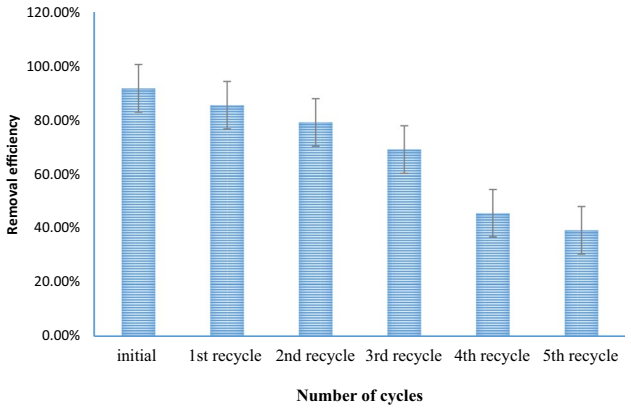

Fig. 16 Adsorbent desorption and its Cr(VI) removal performances

particularly the Box–Behnken design. Four independent factors with levels such as pH (3, 6, and 9), initial Cr(VI) concentrations (40, 70, and 100 mg/L), contact times (30, 60, and 90 min), and adsorbent doses (20, 60, and 100 mg/100 mL) were used. The adsorption main and interaction effects were investigated and their significant influences on the adsorption were recorded. Regarding the adsorbent characterization, FTIR functional groups analysis; the presence of hydroxyl, carboxyl, aldehyde, ketone, and aromatics; BET surface area of 237.4 m^2/g; the predominant peaks of XRD, and SEM analysis of up–down surface morphology were successfully indicated. The adsorption performances of the biochar-magnetite composite for Cr(VI) removals ranged from 17.3 to 91.8% under different treatment conditions. The maximum adsorption performance of the composite adsorbent was found to be 91.8% at the specific experimental condition of the contact time of 90 min, initial Cr(VI) content of 40 mg/L, adsorbent of 100 mg/100 mL, and pH 3, whereas the Cr(VI) removal from real tannery wastewater was 81.8%. Among Langmuir, Freundlich, and Temkin adsorption isotherms, the Langmuir model was the best fit with experimental data at R^2 0.99 and q_{max} 400 mg/g, showing that the adsorption process was homogenous and monolayer. Finally, the adsorption results were encouraging, and biochar–Fe_3O_4 appears to be a potential candidate for Cr removal from tannery wastewater, but further adsorbent potential can be explored through the development of surface multifunctionalities which is essential for scale-up issues at the industrial level.

Acknowledgments We would like to thank the University of South Africa, the Institute for Nanotechnology and Water Sustainability, and Addis Ababa Science and Technology University for the support.

Authors contribution J.F., M.A., and T.N. involved in conceptualization; M.A. and J.F. involved in methodology; M.A. involved in software; J.F. and T.N. involved in validation; J.F. and T.N. involved in formal analysis; M.A. involved in investigation; J.F. and T.N. involved in data curation; J.F., M.A., and T.N. involved in writing—original draft preparation; J.F. and T.N. involved in writing—review and editing; and J.F. involved in visualization and supervision. All authors have read and agreed to the published version of the manuscript.

Funding The author(s) received no specific funding for this work.

Data availability All data are fully available without restriction.

Declarations

Competing interests The authors declare that they have no conflict of interests.

Ethics approval and consent to participate Not applicable.

References

Agra E, Kalderis D, Diamadopoulos E (2014) Arsenic and chromium removal from water using biochars derived from rice husk, organic solid wastes and sewage sludge. J Environ Manage 133:309–314. https://doi.org/10.1016/j.jenvman.2013.12.007

Ahmad W, Qaiser S, Ullah R et al (2021) Utilization of tires waste-derived magnetic-activated carbon for the removal of hexavalent chromium from wastewater. Materials 14:34

Aigbe UO, Osibote OA (2020) A review of hexavalent chromium removal from aqueous solutions by sorption technique using nanomaterials. J Environ Chem Eng 8:104503. https://doi.org/10.1016/j.jece.2020.104503

Alam MS, Bishop B, Chen N et al (2020) Reusable magnetite nanoparticles–biochar composites for the efficient removal of chromate from water. Sci Rep 10:1–12. https://doi.org/10.1038/s41598-020-75924-7

Alzahrani E (2017) Photodegradation of binary azo dyes using core-shell $Fe_3O_4/SiO_2/TiO_2$ nanospheres. Am J Anal Chem 08:95–115. https://doi.org/10.4236/ajac.2017.81008

Ameen A, Saeed H, Harun NY et al (2021) Pristine and magnetic kenaf fiber biochar for Cd^{2+} adsorption from aqueous solution. Int J Environ Res Public Health 18:7949

Aryee AA, Mpatani FM, Du Y et al (2021) Fe3O4 and iminodiacetic acid modified peanut husk as a novel adsorbent for the uptake of Cu (II) and Pb (II) in aqueous solution: characterization, equilibrium and kinetic study. Environ Pollut 268:115729. https://doi.org/10.1016/j.envpol.2020.115729

Badessa TS, Wakuma E, Yimer AM (2020) Bio - sorption for effective removal of chromium (VI) from wastewater using Moringa stenopetala seed powder (MSSP) and banana peel powder (BPP). BMC Chem 14:1–12 https://doi.org/10.1186/s13065-020-00724-z

Baig SA, Zhu J, Muhammad N et al (2014) Effect of synthesis methods on magnetic Kans grass biochar for enhanced As(III, V) adsorption from aqueous solutions. Biomass Bioenerg 71:299–310. https://doi.org/10.1016/j.biombioe.2014.09.027

Bedada D, Angassa K, Tiruneh A et al (2020) Chromium removal from tannery wastewater through activated carbon produced from Parthenium hysterophorus weed. Energy Ecol Environ 5:184–195. https://doi.org/10.1007/s40974-020-00160-8

Bekhoukh A, Moulefera I, Zeggai FZ et al (2022) Anionic methyl orange removal from aqueous solutions by activated carbon reinforced conducting polyaniline as adsorbent: synthesis, characterization, adsorption behavior, regeneration and kinetics study. J Polym Environ 30:886–895. https://doi.org/10.1007/s10924-021-02248-6

Bhushan B, Gupta V, Kotnala S (2020) Materials today: proceedings development of magnetic-biochar nano-composite : assessment of its physico-chemical properties. Mater Today Proc. https://doi.org/10.1016/j.matpr.2020.02.911

Burek P, Satoh Y, Fischer G, et al (2016) Water futures and solution-fasttrack initiative (final report), International institute for applied systems analysis Schlossplatz 1, A-2361 IIASA working paper, Approved by: Bill Cosgrove, Acting program director water, Laxenburg, Austria

Chen C, Chen J, Nguyen N et al (2021) Specifically designed magnetic biochar from waste wood for arsenic removal. Sustain Environ Res 31:1–6

Chen N, Cao S, Zhang L et al (2021) Structural dependent Cr(VI) adsorption and reduction of biochar: hydrochar versus pyrochar. Sci Total Environ 783:147084. https://doi.org/10.1016/j.scitotenv.2021.147084

Cheng N, Wang B, Wu P et al (2021) Adsorption of emerging contaminants from water and wastewater by modified biochar: A review. Environ Pollut 273:116448. https://doi.org/10.1016/j.envpol.2021a.116448

Cheng Y, Chon K, Ren X et al (2021) Bioaugmentation treatment of a novel microbial consortium for degradation of organic pollutants in tannery wastewater under a full-scale oxic process. Biochem Eng J 175:108131. https://doi.org/10.1016/j.bej.2021b.108131

Chowdhury M, Mostafa MG, Biswas TK et al (2015) Characterization of the effluents from leather processing industries. Environ Process 2:173–187

Doumbi RT, Bertrand Noumi G, Ngobtchok B, Domga, (2022) Tannery wastewater treatment by electro-Fenton and electro-persulfate processes using graphite from used batteries as free-cost electrode materials. Case Stud Chem Environ Eng 5:100190. https://doi.org/10.1016/j.cscee.2022.100190

Dudchenko N, Pawar S, Perelshtein I, Fixler D (2022) Magnetite nanoparticles: synthesis and applications in optics. Materials 15:2601

Enaime G, Baçaoui A, Yaacoubi A, Lübken M (2020) Biochar for wastewater treatment-conversion technologies and applications. Appl Sci 10:103492. https://doi.org/10.3390/app10103492

Fito J, Van Hulle SWH (2021) Wastewater reclamation and reuse potentials in agriculture: towards environmental sustainability. Environ Dev Sustain 23:2949–2972. https://doi.org/10.1007/s10668-020-00732-y

Fito J, Tefera N, Van Hulle SWH (2017) Adsorption of distillery spent wash on activated bagasse fly ash: kinetics and thermodynamics. J Environ Chem Eng 5:5381–5388. https://doi.org/10.1016/j.jece.2017.10.009

Fito J, Bultossa G, Kloos H (2019a) Physicochemical and heavy metal constituents of the groundwater quality in Haramaya Woreda, Oromia regional state, Ethiopia. Int J Energy Water Resour 3:23–32. https://doi.org/10.1007/s42108-019-00009-9

Fito J, Said H, Feleke S, Worku A (2019b) Fluoride removal from aqueous solution onto activated carbon of Catha edulis through the adsorption treatment technology. Environ Syst Res 8:1–10. https://doi.org/10.1186/s40068-019-0153-1

Fito J, Abrham S, Angassa K (2020a) Adsorption of methylene blue from textile industrial wastewater onto activated carbon of parthenium hysterophorus. Int J Environ Res 14:501–511. https://doi.org/10.1007/s41742-020-00273-2

Fito J, Abrham S, Angassa K (2020b) Adsorption of methylene blue from textile industrial wastewater onto activated carbon of parthenium hysterophorus. Int J Environ Res. https://doi.org/10.1007/s41742-020-00273-2

Fito J, Kefeni KK, Nkambule TTI (2022) The potential of biochar-photocatalytic nanocomposites for removal of organic micropollutants from wastewater. Sci Total Environ 829:154648. https://doi.org/10.1016/j.scitotenv.2022.154648

Frolova L (2019) Synthesis of magnetic biochar for efficient removal of Cr (III). Adv Mater Sci Eng Hindawi Lond 2019:2987132

Fuat G, Cumali Y (2021) Synthesis, characterization, and lead (II) sorption performance of a new magnetic separable composite: $MnFe_2O_4$@wild plants-derived biochar. J Environ Chem Eng 9:104567. https://doi.org/10.1016/j.jece.2020.104567

Ghasemabadi SM, Baghdadi M, Safari E, Ghazban F (2018) Investigation of continuous adsorption of Pb(II), As(III), Cd(II), and Cr(VI) using a mixture of magnetic graphite oxide and sand as a medium in a fixed-bed column. J Environ Chem Eng 6:4840–4849. https://doi.org/10.1016/j.jece.2018.07.014

Gupta S, Sireesha S, Sreedhar I et al (2020) Latest trends in heavy metal removal from wastewater by biochar based sorbents. J Water Process Eng 38:101561. https://doi.org/10.1016/j.jwpe.2020.101561

Han Z, Sani B, Mrozik W et al (2015) Magnetite impregnation effects on the sorbent properties of activated carbons and biochars. Water Res 70:394–403. https://doi.org/10.1016/j.watres.2014.12.016

Hansen É, Monteiro de Aquim P, Gutterres M (2021) Current technologies for post-tanning wastewater treatment: a review. J Environ Manage 294:113003. https://doi.org/10.1016/j.jenvman.2021.113003

Hoang LP, Van HT, Nguyen LH et al (2019) Removal of Cr(vi) from aqueous solution using magnetic modified biochar derived from raw corncob. New J Chem 43:18663–18672. https://doi.org/10.1039/c9nj02661d

Hoang LP, Nguyen TMP, Van HT et al (2020) Cr(VI) Removal from aqueous solution using a magnetite snail shell. Water Air Soil Pollut 231:63. https://doi.org/10.1007/s11270-020-4406-4

Huang Y, Lee X, Macazo FC et al (2018) Fast and efficient removal of chromium (VI) anionic species by a reusable chitosan-modified multi-walled carbon nanotube composite. Chem Eng J 339:259–267. https://doi.org/10.1016/j.cej.2018.01.133

Ighalo JO, Adeniyi AG (2020) A mini-review of the morphological properties of biosorbents derived from plant leaves. SN Appl Sci 2:1–16. https://doi.org/10.1007/s42452-020-2335-x

Imran M, Haq Khan ZU, Iqbal J et al (2020) Potential of siltstone and its composites with biochar and magnetite nanoparticles for the removal of cadmium from contaminated aqueous solutions: batch and column scale studies. Environ Pollut 259:113938. https://doi.org/10.1016/j.envpol.2020a.113938

Imran M, Ul Z, Khan H et al (2020) Effect of biochar modified with magnetite nanoparticles and HNO_3 for efficient removal of Cr(VI) from contaminated water: a batch and column scale study. Environ Pollut 261:114231. https://doi.org/10.1016/j.envpol.2020.114231

Jahan MAA, Akhtar N, Khan NMS et al (2014) Characterization of tannery wastewater and its treatment by aquatic macrophytes and algae. Bangladesh J Sci Indust Res 49:233–242

Karamipour A, Khadiv Parsi P, Zahedi P, Moosavian SMA (2020) Using Fe_3O_4-coated nanofibers based on cellulose acetate/chitosan for adsorption of Cr(VI), Ni(II) and phenol from aqueous solutions. Int J Biol Macromol 154:1132–1139. https://doi.org/10.1016/j.ijbiomac.2019.11.058

Kong D, He L, Li H et al (2021) Preparation and characterization of graphene oxide/chitosan composite aerogel with high adsorption performance for Cr(VI) by a new crosslinking route. Colloids Surf A Physicochem Eng Asp 625:126832. https://doi.org/10.1016/j.colsurfa.2021.126832

Kosek K, Luczkiewicz A, Fudala-Książek S et al (2020) Implementation of advanced micropollutants removal technologies in wastewater treatment plants (WWTPs)—examples and challenges based on selected EU countries. Environ Sci Policy 112:213–226. https://doi.org/10.1016/j.envsci.2020.06.011

Kosmulski M (2020) The pH dependent surface charging and points of zero charge. VIII. Update. Adv Colloid Interface Sci 275:102064. https://doi.org/10.1016/j.cis.2019.102064

Lee JE, Park YK (2020) Applications of modified biochar-based materials for the removal of environment pollutants: a mini review. Sustain 12:6112. https://doi.org/10.3390/su12156112

Li H, Xiong J, Zhang G et al (2020) Science of the total environment enhanced thallium (I) removal from wastewater using hypochlorite oxidation coupled with magnetite-based biochar adsorption. Sci Total Environ 698:134166. https://doi.org/10.1016/j.scitotenv.2019.134166

Li X, Wang C, Zhang J et al (2020) Preparation and application of magnetic biochar in water treatment: A critical review. Sci Total Environ 711:134847. https://doi.org/10.1016/j.scitotenv.2019.134847

Liang M, Ding Y, Zhang Q et al (2020) Removal of aqueous Cr(VI) by magnetic biochar derived from bagasse. Sci Rep 10:1–13. https://doi.org/10.1038/s41598-020-78142-3

Lingamdinne LP, Roh H, Choi YL et al (2015) Influencing factors on sorption of TNT and RDX using rice husk biochar. J Ind Eng Chem 32:178–186. https://doi.org/10.1016/j.jiec.2015.08.012

Lingamdinne LP, Choi JS, Angaru GKR et al (2022) Magnetic-watermelon rinds biochar for uranium-contaminated water treatment using an electromagnetic semi-batch column with removal mechanistic investigations. Chemosphere 286:131776. https://doi.org/10.1016/j.chemosphere.2021.131776

Liu X, Wang Y, Wang X et al (2022) A salt-free pickling and chrome-free tanning technology: a sustainable approach for cleaner leather manufacturing. Green Chem 24:2179–2192. https://doi.org/10.1039/d1gc04105c

Lyu H, Zhang Q, Shen B (2020) Application of biochar and its composites in catalysis. Chemosphere 240:124842. https://doi.org/10.1016/j.chemosphere.2019.124842

Mallik AK, Moktadir MA, Rahman MA et al (2021) Progress in surface-modified Silicas for Cr(VI) adsorption: a review. J Hazard Mater 423:127041. https://doi.org/10.1016/j.jhazmat.2021.127041

Mishra S, Yadav SS, Rawat S et al (2019) Corn husk derived magnetized activated carbon for the removal of phenol and para-nitrophenol from aqueous solution: interaction mechanism, insights on adsorbent characteristics, and isothermal, kinetic and thermodynamic properties. J Environ Manage 246:362–373. https://doi.org/10.1016/j.jenvman.2019.06.013

Moges A, Nkambule TTI, Fito J (2022) The application of GO-Fe_3O_4 nanocomposite for chromium adsorption from tannery industry wastewater. J Environ Manage 305:114369. https://doi.org/10.1016/j.jenvman.2021.114369

Narasimharao K, Angaru GKR, Momin ZH et al (2023) Orange waste biochar-magnesium silicate (OBMS) composite for enhanced removal of U(VI) ions from aqueous solutions. J Water Process Eng 51:103359. https://doi.org/10.1016/j.jwpe.2022.103359

Narzari R, Poddar MK, Bordoloi N et al (2021) A comprehensive study to understand removal efficiency for Cr6+ using magnetic and activated biochar through response surface methodology. Biomass Convers Biorefinery. https://doi.org/10.1007/s13399-021-01448-3

Navarathna CM, Karunanayake AG, Gunatilake SR et al (2019) Removal of Arsenic (III) from water using magnetite precipitated onto Douglas fir biochar. J Environ Manage 250:109429. https://doi.org/10.1016/j.jenvman.2019.109429

Navarathna CM, Dewage NB, Karunanayake AG et al (2019) Rhodamine B adsorptive removal and photocatalytic degradation on MIL-53-Fe MOF/magnetic magnetite/biochar composites. J Inorg Organomet Polym Mater 30:214–229. https://doi.org/10.1007/s10904-019-01322-w

Neolaka YAB, Lawa Y, Naat JN et al (2020) The adsorption of Cr(VI) from water samples using graphene oxide-magnetic (GO-Fe_3O_4) synthesized from natural cellulose-based graphite (kusambi wood or Schleichera oleosa): study of kinetics, isotherms and thermodynamics. J Mater Res Technol 9:6544–6556. https://doi.org/10.1016/j.jmrt.2020.04.040

Niculescu AG, Chircov C, Grumezescu AM (2022) Magnetite nanoparticles: synthesis methods—a comparative review. Methods 199:16–27. https://doi.org/10.1016/j.ymeth.2021.04.018

Nure JF, Shibeshi NT, Asfaw SL et al (2017) COD and colour removal from molasses spent wash using activated carbon produced from bagasse fly ash of matahara sugar factory, Oromiya region, Ethiopia. Water SA 43:470–479. https://doi.org/10.4314/wsa.v43i3.12

Nur-E-Alam M, Abu Sayid Mia M, Ahmad F, Mafizur Rahman M (2018) Adsorption of chromium (Cr) from tannery wastewater using low-cost spent tea leaves adsorbent. Appl Water Sci 8:1–7. https://doi.org/10.1007/s13201-018-0774-y

Parlayici S, Eskizeybek V, Avc A (2015) Removal of chromium (VI) using activated carbon-supported-functionalized carbon nanotubes. J Nanostruct Chem 5:255–263. https://doi.org/10.1007/s40097-015-0156-z

Pashai M, Milani H, Ghorbani M (2016) Point of zero charge of maghemite decorated multiwalled carbon nanotubes fabricated by chemical precipitation method. J Mol Liq 216:117–125. https://doi.org/10.1016/j.molliq.2015.12.087

Patel H (2021) Review on solvent desorption study from exhausted adsorbent. J Saudi Chem Soc 25:101302. https://doi.org/10.1016/j.jscs.2021.101302

Preethi J, Prabhu SM, Meenakshi S (2017) Effective adsorption of hexavalent chromium using biopolymer assisted oxyhydroxide

materials from aqueous solution. React Funct Polym 117:16–24. https://doi.org/10.1016/j.reactfunctpolym.2017.05.006

Qhubu MC, Mgidlana LG, Madikizela LM, Pakade VE (2021) Preparation, characterization and application of activated clay biochar composite for removal of Cr(VI) in water: isotherms, kinetics and thermodynamics. Mater Chem Phys 260:124165. https://doi.org/10.1016/j.matchemphys.2020.124165

Qu J, Wang Y, Tian X et al (2021) KOH-activated porous biochar with high specific surface area for adsorptive removal of chromium (VI) and naphthalene from water: affecting factors, mechanisms and reusability exploration. J Hazard Mater 401:123292. https://doi.org/10.1016/j.jhazmat.2020.123292

Rajahmundry GK, Garlapati C, Kumar PS et al (2021) Statistical analysis of adsorption isotherm models and its appropriate selection. Chemosphere 276:130176. https://doi.org/10.1016/j.chemosphere.2021.130176

Regkouzas P, Diamadopoulos E (2019) Adsorption of selected organic micro-pollutants on sewage sludge biochar. Chemosphere 224:840–851. https://doi.org/10.1016/j.chemosphere.2019.02.165

Rocha LS, Pereira D, Sousa É et al (2020) Recent advances on the development and application of magnetic activated carbon and char for the removal of pharmaceutical compounds from waters: a review. Sci Total Environ 718:137272. https://doi.org/10.1016/j.scitotenv.2020.137272

Rodr C, Tapia C, Leiva-aravena E et al (2020) Graphene oxide–ZnO nanocomposites for removal of aluminum and copper ions from acid mine drainage wastewater. Int J Environ Res Public Health 17(18):6911

Roh H, Yu MR, Yakkala K et al (2015) Removal studies of Cd(II) and explosive compounds using buffalo weed biochar-alginate beads. J Ind Eng Chem 26:226–233. https://doi.org/10.1016/j.jiec.2014.11.034

Rusmirovic JD, Milo D (2021) Journal of environmental chemical engineering vermiculite enriched by Fe (III) oxides as a novel adsorbent for toxic metals removal. J Environ Chem Eng 9:106020. https://doi.org/10.1016/j.jece.2021.106020

Santhosh C, Daneshvar E, Tripathi KM et al (2020) Synthesis and characterization of magnetic biochar adsorbents for the removal of Cr(VI) and Acid orange 7 dye from aqueous solution. Environ Sci Pollut Res 27:32874–32887. https://doi.org/10.1007/s11356-020-09275-1

Sathish M, Dhathathreyan A, Rao JR (2019) Ultrae ffi cient tanning process: role of mass transfer efficiency and sorption kinetics of Cr(III) in leather processing. ACS Sustain Chem Eng 7:4876. https://doi.org/10.1021/acssuschemeng.8b04876

Sewu DD, Tran HN, Ohemeng-Boahen G, Woo SH (2020) Facile magnetic biochar production route with new goethite nanoparticle precursor. Sci Total Environ 717:137091. https://doi.org/10.1016/j.scitotenv.2020.137091

Shan Y, Yang W, Li Y et al (2019) Preparation of microwave-activated magnetic bio-char adsorbent and study on removal of elemental mercury from flue gas. Sci Total Environ 697:134049. https://doi.org/10.1016/j.scitotenv.2019.134049

Shan H, Zeng C, Zhao C, Zhan H (2021) Iron oxides decorated graphene oxide/chitosan composite beads for enhanced Cr(VI) removal from aqueous solution. Int J Biol Macromol 172:197–209. https://doi.org/10.1016/j.ijbiomac.2021.01.060

Shang J, Pi J, Zong M et al (2016) Journal of the Taiwan institute of chemical engineers chromium removal using magnetic biochar derived from herb-residue. J Taiwan Inst Chem Eng 68:289–294. https://doi.org/10.1016/j.jtice.2016.09.012

Sirajudheen P, Nikitha MR, Karthikeyan P, Meenakshi S (2020) Perceptive removal of toxic azo dyes from water using magnetic Fe_3O_4 reinforced graphene oxide–carboxymethyl cellulose recyclable composite: adsorption investigation of parametric studies and their mechanisms. Surf Interfaces 21:100648. https://doi.org/10.1016/j.surfin.2020.100648

Subedi N, Lähde A, Abu-Danso E et al (2019) A comparative study of magnetic chitosan (Chi@Fe_3O_4) and graphene oxide modified magnetic chitosan (Chi@Fe_3O_4GO) nanocomposites for efficient removal of Cr(VI) from water. Int J Biol Macromol 137:948–959. https://doi.org/10.1016/j.ijbiomac.2019.06.151

Tang Q, Shi C, Shi W et al (2019) Science of the Total Environment Preferable phosphate removal by nano-La (III) hydroxides modified mesoporous rice husk biochars: role of the host pore structure and point of zero charge. Sci Total Environ 662:511–520. https://doi.org/10.1016/j.scitotenv.2019.01.159

Tariq MA, Nadeem M, Iqbal MM et al (2020) Effective sequestration of Cr (VI) from wastewater using nanocomposite of ZnO with cotton stalks biochar: modeling, kinetics, and reusability. Environ Sci Pollut Res 27:33821–33834. https://doi.org/10.1007/s11356-020-09481-x

Tebeje A, Worku Z, Nkambule TTI, Fito J (2021) Adsorption of chemical oxygen demand from textile industrial wastewater through locally prepared bentonite adsorbent. Int J Environ Sci Technol 19:1–14. https://doi.org/10.1007/s13762-021-03230-4

Tsigoida A, Argyrokastritis I (2020) Electrical conductivity, pH and other soil chemical parameters after sub-irrigation with untreated and treated municipal wastewater in two different soils. Glob Nest J 22:55–56. https://doi.org/10.30955/gnj.003217

Ud S, Muhammad D, Khan S et al (2021) Adsorptive mechanism of chromium adsorption on siltstone—nanomagnetite: biochar composite. J Inorg Organomet Polym Mater 31:1608–1620. https://doi.org/10.1007/s10904-020-01829-7

UN-Water (2020) Water and climate change,the united nations world water development report 2020, the United Nations educational, scientific and cultural organization 7. Place de Fontenoy, 75352 Paris 07 SP, France

UN-water (2021) Valuing water,the United Nations world water development report 2021,the United Nations educational, scientific and cultural organization, 7, place de Fontenoy, 75352 Paris 07 SP, France

Vikrant K, Kim KH, Ok YS et al (2018) Engineered/designer biochar for the removal of phosphate in water and wastewater. Sci Total Environ 616–617:1242–1260. https://doi.org/10.1016/j.scitotenv.2017.10.193

Villaseñor-Basulto DL, Picos-Benítez A, Pacheco-Alvarez M et al (2022) Tannery wastewater treatment using combined electrocoagulation and electro-Fenton processes. J Environ Chem Eng 10:107290. https://doi.org/10.1016/j.jece.2022.107290

Waktole Y, Seid B, Mereta T, Fufa F (2019) Simultaneous removal of nitrate and phosphate from wastewater using solid waste from factory. Appl Water Sci 9:1–10. https://doi.org/10.1007/s13201-019-0906-z

Wan J, Liu F, Wang G et al (2021) Exploring different mechanisms of biochars in removing hexavalent chromium: sorption, reduction and electron shuttle. Bioresour Technol 337:125382. https://doi.org/10.1016/j.biortech.2021.125382

Wang J, Wang S (2019) Preparation, modification and environmental application of biochar: a review. J Clean Prod. https://doi.org/10.1016/j.jclepro.2019.04.282

WHO (2012) Water quality for drinking: WHO guidelines. WHO press world heal organ 20 ave Appia, Dordrecht, pp. 876–883 https://doi.org/10.1007/978-1-4020-4410-6_184

Wurzer C, Mašek O (2021) Feedstock doping using iron rich waste increases the pyrolysis gas yield and adsorption performance of magnetic biochar for emerging contaminants. Bioresour Technol 321:124473. https://doi.org/10.1016/j.biortech.2020.124473

WWAP/UN-Water (2017) Wastwater the untapped resource

Xiao Y, Lyu H, Yang C et al (2021) Graphitic carbon nitride/biochar composite synthesized by a facile ball-milling method for the adsorption and photocatalytic degradation of enrofloxacin. J Environ Sci 103:93–107. https://doi.org/10.1016/j.jes.2020.10.006

Yadav A, Raj A, Purchase D et al (2019) Phytotoxicity, cytotoxicity and genotoxicity evaluation of organic and inorganic pollutants rich tannery wastewater from a common effluent treatment plant (CETP) in Unnao district, India using Vigna radiata and Allium cepa. Chemosphere 224:324–332. https://doi.org/10.1016/j.chemosphere.2019.02.124

Yehuala G, Worku Z, Angassa K et al (2021) Electrochemical degradation of chemical oxygen demand in the textile industrial wastewater through the modified electrodes. Arab J Sci Eng. https://doi.org/10.1007/s13369-021-05776-4

Yousefi SR, Ghanbari D, Salavati-Niasari M, Hassanpour M (2016) Photo-degradation of organic dyes: simple chemical synthesis of $Ni(OH)_2$ nanoparticles, Ni/$Ni(OH)_2$ and Ni/NiO magnetic nanocomposites. J Mater Sci Mater Electron 27:1244–1253. https://doi.org/10.1007/s10854-015-3882-6

Yousefi SR, Sobhani A, Salavati-Niasari M (2017) A new nanocomposite superionic system ($CdHgI_4/HgI_2$): synthesis, characterization and experimental investigation. Adv Powder Technol 28:1258–1262. https://doi.org/10.1016/j.apt.2017.02.013

Yousefi SR, Amiri O, Salavati-Niasari M (2019) Control sonochemical parameter to prepare pure $Zn_{0.35}Fe_{2.65}O_4$ nanostructures and study their photocatalytic activity. Ultrason Sonochem 58:104619. https://doi.org/10.1016/j.ultsonch.2019a.104619

Yousefi SR, Masjedi-Arani M, Morassaei MS et al (2019b) Hydrothermal synthesis of $DyMn_2O_5/Ba_3Mn_2O_8$ nanocomposite as a potential hydrogen storage material. Int J Hydrogen Energy 44:24005–24016. https://doi.org/10.1016/j.ijhydene.2019.07.113

Yousefi SR, Alshamsi HA, Amiri O, Salavati-Niasari M (2021) Synthesis, characterization and application of Co/Co_3O_4 nanocomposites as an effective photocatalyst for discoloration of organic dye contaminants in wastewater and antibacterial properties. J Mol Liq 337:116405. https://doi.org/10.1016/j.molliq.2021a.116405

Yousefi SR, Ghanbari M, Amiri O et al (2021b) $Dy_2BaCuO_5/Ba_4DyCu_3O_{9.09}$ *S*-scheme heterojunction nanocomposite with enhanced photocatalytic and antibacterial activities. J Am Ceram Soc 104:2952–2965. https://doi.org/10.1111/jace.17696

Yousefi SR, Sobhani A, Alshamsi HA, Salavati-Niasari M (2021c) Green sonochemical synthesis of $BaDy_2NiO_5/Dy_2O_3$and $BaDy_2NiO_5$/NiO nanocomposites in the presence of core almond as a capping agent and their application as photocatalysts for the removal of organic dyes in water. RSC Adv 11:11500–11512. https://doi.org/10.1039/d0ra10288a

Yu J, Jiang C, Guan Q et al (2018) Enhanced removal of Cr(VI) from aqueous solution by supported ZnO nanoparticles on biochar derived from waste water hyacinth. Chemosphere 195:632–640. https://doi.org/10.1016/j.chemosphere.2017.12.128

Zahedifar M, Seyedi N, Shafiei S, Basij M (2021) Surface-modified magnetic biochar: highly efficient adsorbents for removal of Pb (II) and Cd (II). Mater Chem Phys 271:124860. https://doi.org/10.1016/j.matchemphys.2021.124860

Zahid M, Nadeem N, Hanif MA et al (2019) Metal ferrites and their graphene-based nanocomposites: synthesis, characterization and applications in wastewater treatment. In: Abd-Elsalam KA, Mohamed MA, Prasad R (eds) Magnetic nanostructures: environmental and agricultural applications. Springer International Publishing, Cham

Zhang X, Hao L, Wang H et al (2017) Preparation and characterization of superparamagnetic Fe_3O_4/CNTs nanocomposites dual-drug carrier. J Wuhan Univ Technol Mater Sci Ed 32:42–46. https://doi.org/10.1007/s11595-017-1555-4

Zhang A, Li X, Xing J, Xu G (2020) Adsorption of potentially toxic elements in water by modified biochar: A review. J Environ Chem Eng 8:104196. https://doi.org/10.1016/j.jece.2020.104196

Zhao C, Chen W (2019) A review for tannery wastewater treatment: some thoughts under stricter discharge requirements. Environ Sci Pollut Res 26:26102–26111. https://doi.org/10.1007/s11356-019-05699-6

Zhao C, Yang Q, Chen W, Teng B (2012) Removal of hexavalent chromium in tannery wastewater by Bacillus cereus. Can J Microbiol 28:23–28. https://doi.org/10.1139/W11-096

Zhou R, Jin Y, Lai S et al (2022) A novel composite retanning system based on pH-responsive hydrogen bonding and hydrophobic interaction for cleaner leather processing. J Clean Prod 339:130666. https://doi.org/10.1016/j.jclepro.2022.130666

Zhu S, Huang X, Wang D et al (2018) Chemosphere Enhanced hexavalent chromium removal performance and stabilization by magnetic iron nanoparticles assisted biochar in aqueous solution : mechanisms and application potential. Chemosphere 207:50–59. https://doi.org/10.1016/j.chemosphere.2018.05.046

Zou H, Zhao J, He F et al (2021) Ball milling biochar iron oxide composites for the removal of chromium (Cr(VI)) from water: Performance and mechanisms. J Hazard Mater 413:125252. https://doi.org/10.1016/j.jhazmat.2021.125252

Zubair M, Abdul H, Ihsanullah I (2021) Environmental technology & innovation biochar supported CuFe layered double hydroxide composite as a sustainable adsorbent for efficient removal of anionic azo dye from water. Environ Technol Innov 23:101614. https://doi.org/10.1016/j.eti.2021.101614